Atomization and Sprays, Volume 33, Issue 4, 2023, pp. 25-54
DOI: 10.1615/AtomizSpr.2023041220

VALIDATION OF A STOCHASTIC BREAKUP MODEL FOR TURBULENT JETS IN HIGH-SPEED CROSSFLOW: ASSESSMENT OF TURBULENT INTERACTIONS AND SENSITIVITY TO BOUNDARY CONDITIONS

Malika Zghal[1,], Xiaoxiao Sun[1], Pierre Q. Gauthier[1,2], & Vishal Sethi[1]*

[1] SATM, Cranfield University, Cranfield, Bedfordshire, United Kingdom
[2] Siemens Energy Canada, Montreal, Quebec, Canada

*Address all correspondence to: Malika Zghal, SATM, Cranfield University, Cranfield, United Kingdom, E-mail: m.zghal@cranfield.ac.uk

Improving the mixing of fuel and air by injecting a turbulent liquid fuel jet into a high-speed crossflowing gas can reduce the emissions of gas turbine applications. To facilitate and hasten the development of such low-emissions technologies, accurate predictions of the spray characteristics are needed. The objective of the present study is to validate the predictive capabilities of a stochastic breakup model for turbulent transverse jets over a wide range of representative pressures and atomization characteristics. The effect of turbulence modeling is also assessed to provide accurate and computationally less expensive Eulerian-Lagrangian transient approaches. To do so, the predictions made with the Large Eddy Simulation (LES) approach for different subgrid scale (SGS) models and with the Synthetic Eddy Method (SEM) are compared to the ones made using the unsteady Reynolds-Averaged Navier-Stokes (RANS) approach with and without a turbulent dispersion model. The sensitivity of the numerical methodology to the upstream velocity profile, pressure and momentum flux ratio were also assessed. Properly accounting for the upstream gas velocity profile was found to be critical to ensure accurate predictions of the spray characteristics. The unsteady RANS (URANS) turbulent approach coupled with the turbulent dispersion model showed good agreement with experimental data, but the LES approach tends to overpredict the spray penetration and underpredict the Sauter Mean Diameter (SMD). This could be due to the lower turbulent interactions it predicts, which may lead to lower momentum transfer between the phases.

KEYWORDS: Liquid jet, Crossflow, High pressure, Secondary Breakup, Stochastic, Turbulent dispersion, Simulations, CFD, LES, Unsteady RANS.

1. INTRODUCTION

To address the growing environmental concerns, highly ambitious targets have been set by various legislative bodies to reduce emissions from both stationary and aero gas turbine applications. It is critical to develop more sustainable technologies, such as advanced mixing technologies that reduce emissions by improving the mixing of liquid-fuel sprays with air (Kuo and Acharya, 2012). Once injected in the combustor, the liquid jet is divided into small droplets by going through a primary and secondary breakup process to form a spray that evaporates and mixes with the air. The breakup processes influence the spray characteristics, which significantly influence the combustion process and emissions (Kuo and Acharya, 2012). Mixing can be improved by injecting the liquid fuel transversely into a crossflowing air stream and can be further enhanced by the turbulent characteristics of the liquid jet and air stream (Karagozian, 2010; Mahesh, 2013; Broumand and Birouk, 2016). To facilitate the design work and hasten the delivery of new sustainable technologies, Eulerian and Lagrangian approaches are preferred over the computationally expensive Volume-of-Fluid (VOF) approach. Thus, this study focuses on validating a numerical methodology for turbulent liquid jets in crossflow using a Lagrangian approach.

However, the breakup models used in state-of-the-art CFD are deemed unlikely to be suitable at representative conditions because they are often based on Kelvin-Helmholtz (KH) instabilities growing on the droplet surface (Wave/KH model) (Reitz and Diwakar, 1987), such as the KHRT breakup model (Beale and Reitz, 1999), or on Taylor's analogy (TAB model) (O'Rourke and Amsden, 1987), such as the ETAB breakup model (Tanner, 1997). These use correlations or model constants experimentally determined mainly at atmospheric conditions or without fuel (Li and Soteriou, 2013; Li and Soteriou, 2018). Thus, they need to be calibrated to accurately predict the spray penetration and droplet size distribution (Baumgarten,

Published by Begell House. This is the Author Accepted Manuscript issued with: Creative Commons Attribution Non-Commercial License (CC:BY:NC 4.0).
The final published version (version of record) is available online at DOI:10.1615/AtomizSpr.2023041220. Please refer to any applicable publisher terms of use.

2006; Kuo and Acharya, 2012). Other breakup models developed to improve the predictions in the primary region also require knowledge of the near-field characteristics (Baumgarten, 2006).

The need to generate experimental data to obtain accurate results is counterproductive considering that CFD is used as a tool to guide the design. Thus, numerical models should ideally require minimal calibration. To the best knowledge of the authors, the Madabhushi et al. (2004) breakup model is the only one used in state-of-the-art CFD that has been developed for turbulent jets in crossflow to account for their distinctive characteristics, such as the column bending under aerodynamic forces. However, it also relies on experimental data as it uses the Wave breakup model to account for the primary breakup and other experimental correlations.

The Stochastic Secondary Droplet (SSD) breakup model (Apte et al., 2003) was developed to rely less on experimental data as it considers droplet breakup to be random in nature and to depend more on the boundary conditions by using Kolmogorov's stochastic theory (Apte et al., 2003; Apte et al., 2009). Thus, the breakup is not limited to a single scale and the important processes that occur at the high gas Weber numbers often used in gas turbine applications are captured, such as the effect of turbulence and catastrophic breakup (Apte et al., 2003; Apte et al., 2009). Therefore, the current work studies the predictive capabilities of the SSD model for turbulent jets in crossflow.

Previous studies conducted with the LES and URANS approach showed good agreement between the SSD model and experimental data for different types of coflowing atomizers over a wide range of conditions. However, they noted the SMD tends to be underpredicted regardless of the pressure (Apte et al., 2003; Apte et al., 2009; Nihasigaye and al., 2021) and despite the use of a primary breakup model (Gorokhovski et al., 2012; Nihasigaye and al., 2021). To the best knowledge of the authors, previous studies on the SSD model with a jet in crossflow configuration were limited to ambient pressure and low gas Weber numbers (Herrmann, 2009), used water (Herrmann, 2009; Bravo et al., 2018) or used either non-turbulent jets (Bravo et al., 2018) or a very low momentum flux ratio (Herrmann, 2009). Moreover, they mostly focused on assessing the predictive capabilities in the primary breakup region with a hybrid VOF-Lagrangian approach (Herrmann, 2009; Bravo et al., 2018), which is not where the SSD model dominates. Regarding turbulence modeling, Apte et al., (2009) obtained good agreement for coflowing sprays between URANS and LES with a dynamic subgrid-scale model but recommended the use of additional models for the RANS turbulence approach due to disparities observed in the far-field region. Heide et al. (2017) concluded that such additional turbulence models were necessary for coflowing sprays to obtain accurate trajectory predictions in the near-field region. Blanchard and Shi (2012) explored reducing the computational cost by using RANS simulations with a turbulent dispersion model. However, the effects of the latter were not assessed as it focused more on the effect of modeling droplet collision and coalescence, which was found necessary to avoid SMD underprediction.

Furthermore, most numerical studies on jets in crossflow assume a constant gas velocity profile as they consider the difference between the mean and peak velocity to be negligible (Behzad et al., 2016; Wen et al., 2020). Many experimental studies (Stenzler and Santavicca, 2003; Bellofiore et al., 2005; Lubarsky et al., 2010; Lubarsky, et al., 2011; Farvardin et al., 2013) interpret the velocity profile as flat despite a thick boundary layer measured or the use of a long flow straightening channel since achieving it used to be a popular design criterion. Meanwhile, other research reporting similar velocity profiles (Becker and Hassa, 2002; Brown et al., 2007; Li et al., 2012; Amighi 2015; Song et al., 2019) have a different interpretation despite the similar experimental setup and often use the mean velocity to extract an experimental correlation. However, the experimental test sections commonly used are usually small (a few millimeters) and only one order of magnitude higher than the boundary layer thickness. Thus, the effect of the latter on the flow field could be important. To the best knowledge of the authors, the effect of assuming a constant gas velocity profile on the spray predictions has not been assessed yet.

Therefore, the objective of this study is to answer the need of validating the predictive capabilities of the SSD breakup model at more representative gas turbine conditions for turbulent liquid jets in crossflow. The

effect of additional turbulence modeling on less computationally expensive Eulerian-Lagrangian transient approaches is also assessed to provide fast and accurate design tools. To do so, the effects on the LES predictions of different subgrid-scale models and of using turbulent boundary conditions through the Synthetic Eddy Method are compared to the effect on the URANS predictions of using a turbulent dispersion model. The results are validated against experimental data available in the literature over a wide range of conditions. The sensitivities of the numerical approach to the velocity profile, pressure and momentum flux ratio are also studied.

2. GOVERNING EQUATIONS

With the Lagrangian-Eulerian approach, a discrete element type of method is used to track clusters of particles with identical properties inside the computational domain and to solve governing equations for their instantaneous state as described by Crowe (1998). Using a statistical approach by solving the Lagrangian equations for parcels of particles reduces the computational cost.

2.1 LAGRANGIAN FRAMEWORK

The interactions between the dispersed and continuous phases are modeled through two-way coupling, which considers the influence of the gas on the droplets as well as the opposite. In the present work, heat and mass transfer were neglected due to the negligible temperature differential as presented in section 3. Therefore, the interactions are modelled by only considering the transfer of momentum and energy by applying as a source term the resulting net exchanges to the corresponding governing equation of the continuous phase. For each cell, the net exchange of all particles crossing its volume is obtained by summing-up the change of each particle. These are calculated by integrating the dispersed phase equations over the cell. The resulting transfer rates of momentum S_v and energy S_E to the continuous phase are defined as (Simcenter STAR-CCM+)

$$S_v = -\frac{1}{\Delta t}\sum_{\pi}\sum_{\delta t_p} n_\pi (F_s)\delta t_p \tag{1}$$

$$S_E = -\frac{1}{\Delta t}\sum_{\pi}\sum_{\delta t_p} n_\pi (F_s \cdot u_p)\delta t_p \tag{2}$$

Where n_π is the number of particles within a parcel, Δt the physical time-step, δt_p the local parcel time-step and u_p the particle velocity. The surface force applied on the droplets F_s represents the aerodynamic effects and pressure changes in the continuous phase and is calculated as

$$F_s = F_d + F_p \tag{3}$$

Where F_d is the drag force and F_p the pressure gradient force, which is defined as

$$F_p = -V_p \nabla P_{static} = -\left({}^{m_p}/_{\rho_p}\right)\nabla P_{static} \tag{4}$$

Where m_p is the particle mass, V_p the particle's volume, ρ_p the particle's density and ∇P_{static} the static pressure gradient of the continuous phase. The drag force in Eq.(3) is defined as

$$F_d = \frac{1}{2} C_D \rho A_p |u_s| u_s = \left(m_p u_s\right)/\tau_v \tag{5}$$

Where C_D is the drag force coefficient, ρ the continuous phase's density, A_p the particle's projected area, τ_v the momentum-relaxation time scale and u_s the particle's slip velocity calculated as

$$u_s = u - u_p \tag{6}$$

Where u is the velocity of the continuous phase. The motion of the particle due to the forces acting on its surface is defined by the equation of the conservation of the translational momentum

$$m_p \frac{du_p}{dt} = F_s \tag{7}$$

Integrating over time the particle's equation of motion described in Eq.(7) gives the particle's instantaneous velocity u_p. Integrating the latter over time gives the particle's instantaneous position vector R_p, which once integrated over time gives the particle's trajectory. Within a time-step Δt of the unsteady solver, the solution of each parcel is time-marched every inner iteration by the Lagrangian solver through an adaptive

local parcel time-step δt_p. The temporal error is controlled through the latter by restricting its value to (Simcenter STAR-CCM+)

$$\frac{Co_{min}\Delta x}{\max(|u|,|u_p|)} \leq \delta t_p \leq \frac{Co_{max}\Delta x}{\max(|u|,|u_p|)} \quad where\ \delta t_p \leq \Delta t \tag{8}$$

Where Co_{max} and Co_{min} are the maximum and minimum Lagrangian phase courant numbers and Δx is a characteristic length of the cell. A smaller time-step and Lagrangian courant numbers increase the accuracy of the solution at the expense of computational time.

2.2 DRAG FORCE & TAB DISTORTION

The Liu Dynamic drag coefficient C_D defined in Eq.(9) accounts for the droplet's deformation due to the surrounding aerodynamic forces (Liu et al., 1993) through the TAB distortion model, which considers it to be analogous to a damped spring-mass system where breakup occurs at a critical oscillation frequency characterized by a critical gas Weber number (O'Rourke and Amsden,1987).

$$C_D = C_{D,sphere}(1 + 2.632y) \tag{9}$$

Where $C_{D,sphere}$ is the drag coefficient of an undistorted droplet defined by (Amsden et al., 1985)

$$C_{D,sphere} = \begin{cases} \frac{24}{Re_p}\left(1 + \frac{1}{6}{Re_p}^{2/3}\right) & Re_p \leq 1000 \\ 0.424 & Re_p > 1000 \end{cases} \tag{10}$$

Where Re_p is the particle's Reynolds number as calculated by

$$Re_p = \left(\rho_p |u_s| D_p\right)/\mu_p \tag{11}$$

Where μ_p is the particle dynamic viscosity and D_p the particle diameter. The normalized droplet distortion y is calculated by analytically solving a second order ODE function of the gas Weber number calculated as

$$We = \left(\rho |u_s|^2 D_p\right)/\sigma \tag{12}$$

Where σ is the surface tension. The value of the normalized distortion y is 0 when the droplet is spherical, and 1 when the droplet is completely distorted.

2.3 SSD BREAKUP MODEL

The Stochastic Secondary Droplet (SSD) breakup model (Apte et al., 2003) is based on the stochastic Lagrangian breakup model first proposed by Gorokhovski and Saveliev (2003). It considers the secondary breakup process to be a discrete random occurrence independent of the parent droplet diameter. To do so, it uses a reformulation of Kolmogorov's stochastic theory where the breakup process is asymptotically reduced to the Fokker-Planck differential equation (Apte et al., 2003; Gorokhovski and Saveliev, 2003). Within each parcel where breakup is predicted to occur, the diameters of the child droplets are sampled according to the log-normal distribution obtained by analytically solving the Fokker-Planck differential equation for the droplet diameter probability density function (Apte et al., 2003; Gorokhovski and Saveliev, 2003). The SSD model considers the secondary breakup process depends on the aerodynamic and surface tension forces acting on the droplet's surface. Hence, the temporal evolution of the distribution function is governed by the local flow characteristics and its parameters are given as a function of the parent droplet Weber number (Apte et al., 2009). With the SSD model, two criteria must be met for secondary droplet breakup to occur. The droplet surface must first be unstable, which occurs when the parent droplet radius is bigger than a critical radius defined as

$$r_c = \frac{(We_{crit}\sigma)}{\rho {u_s}^2} \tag{13}$$

When the droplet radius is equal to the critical droplet radius r_c, the SSD model considers that the hydrodynamic forces are balancing the capillary forces, which makes the droplet on the verge of becoming unstable (Apte et al., 2003). Thus, a droplet with a larger radius is considered subjected to a force imbalance, which causes the droplet's surface to become unstable and makes it prone to breakup. The droplet Weber

number must also be bigger than a critical value, which was assumed equal to 6 based on the linear stability analyses of the related experimental correlation (Pilch and Erdman, 1987). Secondly, the local residence time in the computational domain of an unstable droplet must be larger than its breakup time, which is calculated as (Simcenter STAR-CCM+)

$$\tau_{bu} = B_1\sqrt{\rho_p/\rho}\,(r_p/u_s) \tag{14}$$

Decreasing the model constant B_1 increases droplet breakup because it reduces the breakup time. When both droplet breakup conditions are met, the parent droplet is replaced by child droplets. For the statistical approach of the Lagrangian framework, breakup occurs when the identical droplets contained within a parcel meet the breakup conditions of the SSD model. The parent parcel disappears after it breaks up into a number of child parcels that each contains identical child droplets that can cause further breakup if they meet the breakup conditions. The diameter of the child droplets contained within the child parcels is obtained by sampling the log-normal size-distribution function

$$\Phi(r_{p,c}) = \frac{1}{2}\left(1 + erf\left[\frac{log(r_{p,c}/r_p) - \langle\xi\rangle}{\sqrt{2\langle\xi^2\rangle}}\right]\right) \tag{15}$$

Where $r_{p,c}$ is the radius of the child particle, r_p is the radius of the parent particle, $\langle\xi\rangle$ is the first logarithmic moment of the breakup spectrum function and $\langle\xi^2\rangle$ is the second logarithmic moment, which can be interpreted as indicators of its mean value and variance respectively. Further details on the equations and effects of the parameters from the SSD breakup model can be found in Apte et al. (2003; 2009) and references therein. Although the SSD model considers the droplet size distribution function to be independent of the parent droplet diameter, it is included as a parameter in Eq.(15) to set the upper limit of the child droplet diameter range. The lower limit corresponds to half the critical diameter. The mean value of the breakup distribution function is defined as

$$\langle\xi\rangle = K_0 \tag{16}$$

Where K_0 is a model constant of default value -0.1. Increasing its value increases the mean diameter of the child parcels. The variance of the droplet diameter distribution is defined as

$$\langle\xi^2\rangle = K_1 \ln(We/We_{crit}) \tag{17}$$

Where K_1 is a model constant with the default value of 0.1. Increasing its value or the Weber number increases the variance of the size-distribution, causing the child droplet diameters to deviate more from the mean value of the distribution. Due to the nature of the breakup process, the child droplets are assumed to gain momentum in the direction normal to the slip velocity vector, which is accounted for by applying a multiplication factor $|W_{bu}|$ to the inherited parent droplet velocity. Since this multiplication factor considers the child droplets size, their velocity $u_{p,c}$ can only be calculated once their diameter is obtained from Eq.(15) and is then defined as

$$u_{p,c} = |W_{bu}|u_p = \left(K_3 r_{p,c}/\tau_{bu}\right)u_p \tag{18}$$

Where K_3 is a normal velocity coefficient impacting the spray angle with a value limited between 0 and 1. Increasing its value increases the radial diffusion of the spray.

2.4 TURBULENT DISPERSION

Particles traveling through a turbulent flow field are assumed to interact with turbulent eddies, which subjects them to a randomly fluctuating flow field that modifies their respective trajectories following the principle of inertia. To capture the resulting higher level of droplet dispersion, the effect of the turbulent eddies must be included along with the aerodynamics effects. For many flow applications, the LES approach accounts for the turbulent interactions more accurately than the RANS approach (Wang and Squires, 1996; Ničeno et al., 2008). However, as further discussed in section 4.1.4, this is not the case when the unresolved small-scale motions could have a significant impact on the physical process modeled (Wang and Squires, 1996; Gorokhovski and Oruganti, 2021). In the present study, the baseline predictive capabilities of LES for turbulent jets in high-speed crossflow are compared to the unsteady RANS approach with and without the use of a stochastic model that better accounts for the turbulent interactions.

The Turbulent Dispersion model adapted from Gosman and Ioannides (1981) can be added to the Eulerian-Lagrangian Framework to improve the turbulence modeling of the unsteady RANS approach. With the latter, turbulence is modelled through a turbulent eddy viscosity applied to a time-averaged flow field. A stochastic method based on the phase interaction model developed by Dukowicz (1980) is used to include the effect of the instantaneous velocity field fluctuating under the disruptions caused by turbulent eddies, which is calculated as

$$u = \bar{u} + u' \tag{19}$$

Where $\bar{u}$ is the local Reynolds-averaged velocity and u' is the fluctuating eddy velocity, which is calculated using a normal Gaussian. The fluctuating eddy velocity is applied to the Reynolds-Averaged flow while the droplet interacts with the eddy, which ends when the lifetime of the eddy is reached, or when the distance between both of them exceeds the eddy length scale. This eddy interaction time τ_l is defined as (Brown and Hutchinson, 1979)

$$\tau_l = \min(\tau_e, \tau_c) \tag{20}$$

Where τ_c is the eddy transit time and τ_e the eddy time scale representing its lifetime and given by

$$\tau_e = \frac{2\mu_t}{\rho {u_e}^2} = \frac{3\mu_t}{\rho k} \tag{21}$$

Where μ_t is the turbulent eddy viscosity, k the turbulent kinetic energy and u_e the eddy velocity scale. The eddy transit time, which represents the time it takes for the droplet to be separated from the eddy by a distance larger than its length, depends on the aerodynamic forces and is defined as

$$\tau_c = \begin{cases} \infty & \tau_v \leq l_e/|u_s| \\ -\tau_v \ln\left(1 - \dfrac{l_e}{\tau_v |u_s|}\right) & \tau_v > l_e/|u_s| \end{cases} \tag{22}$$

Where τ_v is the momentum relaxation time scale in Eq.(5) and l_e the eddy length scale defined as

$$l_e = u_e \tau_e = \left({}^{2\mu_t}/_{\rho}\right)\sqrt{3/(2k)} \tag{23}$$

The eddy velocity scale, which represents the standard deviation of the eddy velocity fluctuation, is calculated as

$$u_e = \left({}^{l_t}/_{\tau_t}\right)\sqrt{2/3} = \sqrt{(2k)/3} \tag{24}$$

Where l_t is the turbulent length scale and τ_t the turbulent time scale. The definition of the turbulent time scale, velocity scale, kinetic energy and viscosity depend on the turbulence model used.

2.5 RANS TURBULENCE MODELING

For the URANS simulations, turbulence is modeled using the realizable k-epsilon two-layer model, which applies the two-layer approach (Rodi, 1991) to the realizable k-epsilon model and allows to use an all y+ wall treatment. The turbulent length and time scales are calculated as

$$\tau_t = k/\varepsilon \tag{25}$$

$$l_t = \tau_t \sqrt{k} \tag{26}$$

The dissipation rate ε and the turbulent kinetic energy are obtained through the realizable k-epsilon transport equation (Shih et al. 1995). With the two-layer model, the turbulent dissipation rate and turbulent viscosity near the wall are prescribed by the Wolfstein (1969) formulations. The turbulent viscosity is calculated considering the applicability limit of the two-layer formulation through a wall-proximity indicator (Jongen, 1998), which blends the turbulent viscosities of the two-layer model and realizable k-epsilon model. The formulation of the latter is similar to the standard k-epsilon model, but it applies a damping factor that is function of the mean strain rate and vorticity tensors. The turbulent viscosity is used to compute the viscous stress tensor, which is added to the stress tensor used in the RANS transport equations to effectively close them.

2.6 LES TURBULENCE MODELING

For LES, the smaller scales are implicitly filtered by accounting for the subgrid-scale (SGS) interactions through a stress tensor described by the Boussinesq approximation. It is then added to the stress tensor used in the filtered transport equations to effectively close them. In the present work, the WALES SGS model with a length scale limit applied (Nicoud and Ducros, 1999) and the Smagorinsky (1963) SGS model with a standard Van Driest (1956) damping function are used with their standard model constant. Once the turbulent SGS viscosity is obtained, the LES approach prescribes an algebraic formulation to compute the related SGS turbulent kinetic energy and dissipation rate, which are defined as (Vreman et al., 1994)

$$k_{SGS} = C_t S(\mu_t/\rho) = C_t S(\Delta^2 S_{SGS}) \quad (27)$$

$$\varepsilon_{SGS} = S^2(\mu_t/\rho) = S^2(\Delta^2 S_{SGS}) \quad (28)$$

Where C_t is a model constant equal to 3.5 and Δ is the grid filtered width. For the WALES SGS model, S_{SGS} is a deformation parameter computed from the resolved velocity and from the mean strain rate tensor S. For the Smagorinsky SGS model, it corresponds to the latter. The SGS values are used in Eq.(25) and Eq.(26) to obtain the SGS turbulent time and length scales.

3. COMPUTATIONAL SET-UP

3.1 NUMERICAL DOMAIN, MESH AND BOUNDARY CONDITIONS

Experimental datasets at standard temperature and high-pressure using Kerosene fuel from Freitag and Hassa (2008) were used to validate the predictions in jet trajectory at high pressure (case 1-2 P_g=4 bar, case 3 P_g=8bar), high gas Weber number (case 1-2 We_g=586, case 3 We_g=1172) and high droplet gas Reynolds number (case 1-2 $Re_{g,d}$=9.2E+03, case 3 $Re_{g,d}$=1.8E+03). The datasets at standard temperature and pressure using Jet-A fuel from Madabhushi et al. (2004) (We_g=720, $Re_{g,d}$=7.8E+03) were used to assess the predictions for the Sauter Mean Diameter (SMD) at high jet Weber number We_j and jet Reynolds number Re_j, which are compared in **Table 1**. Madabhushi et al. (2004) also developed a breakup model specifically for jets in crossflow and their numerical predictions will be compared. These datasets can also be characterized by their momentum flux ratio *J*, which is initially calculated as

$$J = (\rho_j u_j{}^2)/(\rho_g u_g{}^2) \quad (29)$$

Where u_j is the initial jet velocity, u_g the mean gas velocity upstream of the injector, and ρ_j and ρ_g the initial jet and gas density. A higher value of *J* results in a higher spray trajectory (Broumand and Birouk, 2016). A previous parametric study of the SSD breakup model using similar datasets was conducted by the authors (Zghal et al., 2022). The numerical domains lengths and mesh settings used are imposed in the present study. The experimental cross-section dimensions were imposed to the numerical domains shown in **Figure 1**.

Table 1: Experimental flow properties used for the numerical operating conditions

Datasets	Madabhushi et al. (2004)	Freitag and Hassa (2008)		
		case 1	case 2	case 3
u_j [m/s]	31	13.9	27.9	19.7
u_j/u_g	0.22	0.19	0.37	0.26
J	33.6	6	24	6
We_j	2.47E+04	3.52E+03	1.41E+04	7.03E+03
Re_j	1.18E+04	3.70E+03	7.39E+03	5.23E+03

For the boundary conditions, an inlet velocity profile is imposed, and adiabatic no-slip walls are used. For the datasets of Freitag and Hassa (2008), an unsteady non-reflecting condition is imposed at the pressure outlet to prevent non-physical acoustic reflections. The injection is done in the middle, downstream of the air inlet to achieve an established flow field in the spray region. Because both experiments used plain orifice injectors, the parcel streams were injected with droplets initially at the size of the nozzle diameter *d*, which corresponds to 0.762mm and 0.5mm for the dataset from Madabhushi et al. (2004) and Freitag and Hassa (2008) respectively.

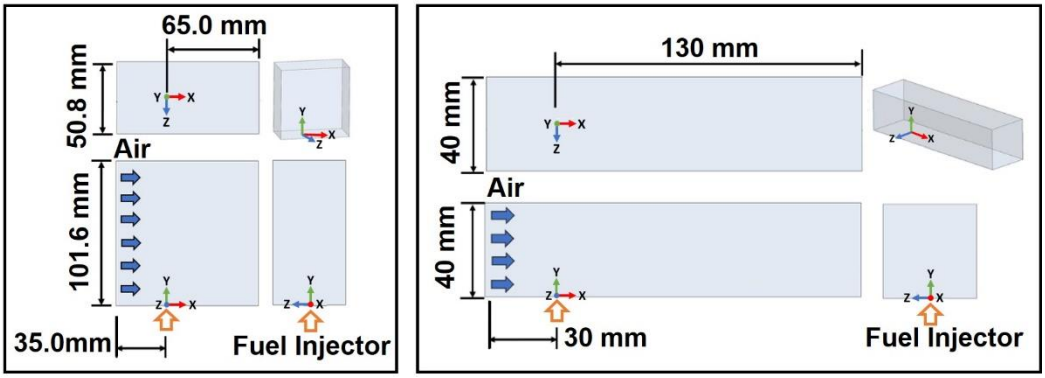

Figure 1: Numerical domain used for the assessment done using the datasets from Madabhushi et al. (2004) [right] and Freitag and Hassa (2008) [left].

For all simulations, the mesh is made of polyhedral cells with the same parameters, which were selected following a mesh refinement study using the dataset from Madabhushi et al. (2004). The volume mesh was refined to 0.4mm in the near-field region and to 0.45mm in the far-field region. The resulting mesh has 3.4 million elements for the numerical domain of Madabhushi et al. (2004) and 2.8 million elements for Freitag and Hassa (2008). The mesh was made fine enough for LES to obtain a courant number near or below unity in the spray and wall y+ values below 2.

3.2 FULLY DEVELOPED TURBULENT VELOCITY PROFILE CORRELATION

Using a correlation to predict the turbulent gas velocity profile would reduce the computation time from having to obtain it numerically. The empirical power-law velocity profile correlation for fully developed turbulent flow in circular pipes was adapted for rectangular ducts by Peszyński (2019)

$$u(x,y) = u_c\left(1-(x/0.5W)\right)^{1/n}\left(1-(y/0.5H)\right)^{1/n} \quad (30)$$

Where x and y are the horizontal and vertical coordinate in the rectangular cross-section, W the width, H the height, n a model constant function of the hydraulic Reynolds number and u_c the centerline velocity calculated as (Munson et al., 2006)

$$u_c = u(n+1)(2n+1)/2n^2 \quad (31)$$

The correlation was validated for both datasets by performing URANS simulations with the turbulent dispersion model. The calculated fully developed turbulent velocity profile was imposed at the inlet of the domain in **Figure 1** by using Eq.(30) with over 3000 (x,y) coordinates. For the conditions of Freitag & Hassa (2008), the constant n was set to 7, which is also the standard value used by the power-law velocity profile that gives reasonable results for many flows application (Munson et al., 2006). For the conditions of Madabhushi et al. (2004), a value of 9 was found to agree well with the experimental one, which is more flat-shaped. The resulting predictions were compared to those obtained with a numerically fully developed turbulent velocity profile. To obtain the latter, RANS simulations of the numerical domains elongated to a length superior to a calculated entrance length were performed with a constant inlet velocity profile. The resulting outlet velocity profile was then imposed at the inlet of the shorter domain for the URANS study. The spray characteristics obtained using both velocity profiles were found to agree well together and with the experimental data. Indeed, they did not predict any significant differences in SMD or maximum spray trajectory for the conditions of Freitag & Hassa (2008) case 1 and Madabhushi et al. (2004). Thus, Eq.(30) was used to assess the sensitivity of the numerical methodology to the inlet velocity profile.

Preliminary studies were conducted using these results to determine which profile to use for the baseline assessments of the turbulence approaches. For the dataset from Madabhushi et al. (2004), a constant velocity profile (u_g=138m/s) is imposed due to the better agreement with the experimental one. For the dataset from Freitag & Hassa (2008), a fully developed velocity profile is imposed due to the better agreement with the experimental maximum jet trajectory compared to a constant velocity profile (u_g=75m/s) as further discussed in Section 4.4 and Section 4.6.

3.3 PHYSICS MODEL

The simulations conducted using Simcenter STAR-CCM+ 2020.3 are three-dimensional, adiabatic, compressible using ideal gas, turbulent and use the implicit unsteady solver with a second-order temporal discretization. For URANS, the coupled energy and flow models with a second-order discretization scheme are used to improve the phase coupling. The realizable k-epsilon two-layer turbulence model is used with a two-layer all y+ wall treatment. For LES, the segregated energy solver with a bounded-central convection scheme and the segregated fluid temperature model with second-order convection are used with an all y+ wall treatment. The Smagorinsky and WALES SGS models are compared, and the impact of turbulent boundary conditions is studied using the Synthetic Eddy Method (SEM) with an assumption of isotropy. For the Lagrangian phase, a two-way coupling approach is used with the SSD breakup model coupled with the TAB distortion model for the drag coefficient. The model constants B_1 and K_3 were respectively imposed equal to $\sqrt{3}$ and 1, which have been shown to improve the SMD predictions and enhance the spray radial diffusion (Zghal et al., 2022).

A preliminary parametric study using the URANS approach was done with the datasets from Madabhushi et al. (2004) to assess the effect of the target number of particles per parcel and number of parcels. Increasing their values can reduce the statistical error by improving the spray discretization, but at the expense of increasing the computational cost (Simcenter STAR-CCM+). It confirmed that these parameters do not affect the droplet characteristics but tend to impact the spray width and jet trajectory. Because the datasets from Freitag and Hassa (2008) are used to assess the latter, the target number of particles per parcel and number of parcel streams are imposed to higher values of 200 and 500 respectively. For the datasets of Madabhushi et al. (2004), they are both set to 100. The maximum number of child parcels is set to 10.

The Lagrangian Courant numbers are imposed to respect the restrictions on the local parcel time-step δt_p defined in Eq.(8) and its maximum is limited by the solution time-step according to

$$Co_{max} \leq \max(|u|, |u_p|)\, \Delta t/\Delta x \tag{32}$$

To determine the smallest value of Co_{max} required to be suitable for the entire spray, u_p was set equal to u_j, u to the minimum value between the volume average and maximum velocity in the domain prior to any injection and Δx to the maximum cell size in the spray region. Co_{min} was then set to a smaller value. The values of Co_{max} and Co_{min} were inferior to 0.25 and 0.1 respectively.

For URANS, the constant CFL number was selected to ensure stable convergence. The time-step Δt was set to 1µs and the numbers of inner iterations were selected to ensure a minimum convergence to the 2nd or 3rd order of magnitude. For LES, more than 80% of the turbulent kinetic energy spectrum was resolved in the spray.

3.4 POST-PROCESSING METHODOLOGY

All values presented (axial evolutions, centerline profiles, contours, etc.) are time-averaged over at least twice the residence time. The properties of the continuous phase (u, ρ, k, μ_t) and parameters that depend only on them (τ_e, u_e, l_e) are volume-averaged unless otherwise specified. The properties of the dispersed phase (u_p, ρ_p, m_p) and related parameters (u_s, τ_v) are particle-averaged unless otherwise specified. The parameters depending on both phases (J_{Local}, τ_c) are calculated using a combination of volume-averaged and particle-averaged values. They are assessed within the spray region by using a volume threshold of the droplets. Their axial evolution is obtained by dividing the latter into sections of equal width (Δx=2mm) and evaluating their values within each section.

To assess the turbulent interactions, the eddy time and length scales, eddy transit and interaction times are calculated using the expressions of the turbulent dispersion model defined in section 2.4. For LES, the resolved turbulent kinetic energy is obtained by summing up half of the velocity components variance. To assess the phase interactions, the net momentum transfer rate is obtained from Eq.(1) through a volume-summation as described in section 2.1. The cumulative curves are then obtained by successively summing up the net momentum transfer rate within each volume sections. The local momentum flux ratio J_{local} across

the spray is also analyzed using Eq.(29) by replacing u_j with the vertical component of the droplet velocity u_{pj} and u_g by the local value u. It is then normalized by the imposed momentum flux ratio J presented in **Table 1.**

The spray trajectories predicted are obtained by evaluating the droplets' maximum vertical position within each volume section. For the datasets from Freitag and Hassa (2008), they are compared to those obtained with their empirical correlation derived from the same experiments as presented in **Table 2**. For the dataset from Madabhushi et al. (2004), empirical correlations available in the literature obtained using similar datasets of liquid-fuel jets in crossflow inside a rectangular channel under standard pressure and temperature are used. The correlation from Becker and Hassa (2002) and Farvardin et al. (2013) were selected as their ranges of momentum flux ratios cover its conditions. The correlation from Tambe et al. (2005) was selected due to its range of nozzle diameters, Re_j and We_g. The latter is also true for Becker and Hassa (2002).

Table 2: Empirical correlations for the maximum spray trajectory

Reference	Liquid	*Y/d*
Freitag and Hassa (2008)	Kerosene	$1.6\mathrm{LN}(3.81(x/d)+1)J^{0.4}$
Becker and Hassa (2002)	Jet-A-1	$1.48\mathrm{LN}(3.56(x/d)+1)J^{0.42}$
Farvardin et al. (2013)	Diesel, Diesel blends	$3.688J^{0.430}(x/d)^{0.384}We_g{}^{-0.085}\left(\mu_j/\mu_{H2O}\right)^{-0.222}$
Tambe et al. (2005)	Jet-A, Water, N-Heptane	$1.55\mathrm{LN}(1.66(x/d)+1)J^{0.53}$

The contours presented are on a middle (z=0) XY cross-section plane and the spray characteristics shown are mapped on the continuous phase. The centerline profile (z=0) for the SMD, gas velocity and droplet velocity are assessed at a YZ cross section plane where there are discrepancies in spray trajectories between URANS and LES. The normalized position of x/d≈33 was selected for both datasets as it allows to compare the predicted SMD with the data from Madabhushi et al. (2004). The SMD is calculated as (Lefebvre and McDonell, 2017)

$$\mathrm{SMD} = \left(\sum n_\pi {D_p}^3\right)/\left(\sum n_\pi {D_p}^2\right) \tag{33}$$

4. RESULTS

An assessment of the turbulence approaches (LES, URANS, turbulent dispersion) is first carried out using case 1 from Freitag and Hassa (2008) and the dataset from Madabhushi et al. (2004) with a fully developed and constant velocity profile respectively. The sensitivity to the inlet velocity profile is then studied by imposing the opposite velocity profile. The sensitivity to the boundary conditions and velocity profile is further analyzed with the datasets from Freitag & Hassa (2008).

4.1 URANS VS LES: EFFECT ON PREDICTIONS

The predictive capabilities of URANS and LES for different SGS models and SEM are compared. The discrepancies are explained by analyzing the momentum transfer and turbulent interactions.

4.1.1 URANS VS LES: TRAJECTORY PREDICTIONS

For the datasets of Freitag and Hassa (2008), LES tends to predict a higher maximum spray trajectory compared to the experimental correlation and to URANS after the primary breakup region ($x/d \geq 10$) as seen in **Figure 2**. Indeed, it predicts a spray trajectory on average 17% higher than URANS and an average relative error with the data of 25% compared to 7% for URANS. Moreover, URANS yields better agreement with the data on a longer axial distance ($x/d \leq 50$).

The predictions obtained with the dataset from Madabhushi et al. (2004) indicate that LES tends to overpredict the trajectory regardless of the conditions. Indeed, it predicts an average relative error of 40%, 20.5% and 13% with the experimental correlation of Becker et Hassa (2002), Farvardin et al. (2013) and

Tambe et al. (2005) respectively, compared to 37%, 19% and 11% for URANS. However, the difference with URANS is less significant as LES predicts it higher by 3.5% at most. Moreover, the predictions are similar on a longer axial distance ($x/d \leq 30$) compared to the dataset of Freitag and Hassa (2008) ($x/d \leq 10$). This could indicate that the trajectory predicted by URANS is sensitive to the boundary conditions. To determine if this is caused by the lower pressure or higher momentum flux ratio used, further studies were done with the datasets from Freitag & Hassa (2008) as discussed in Section 4.6.

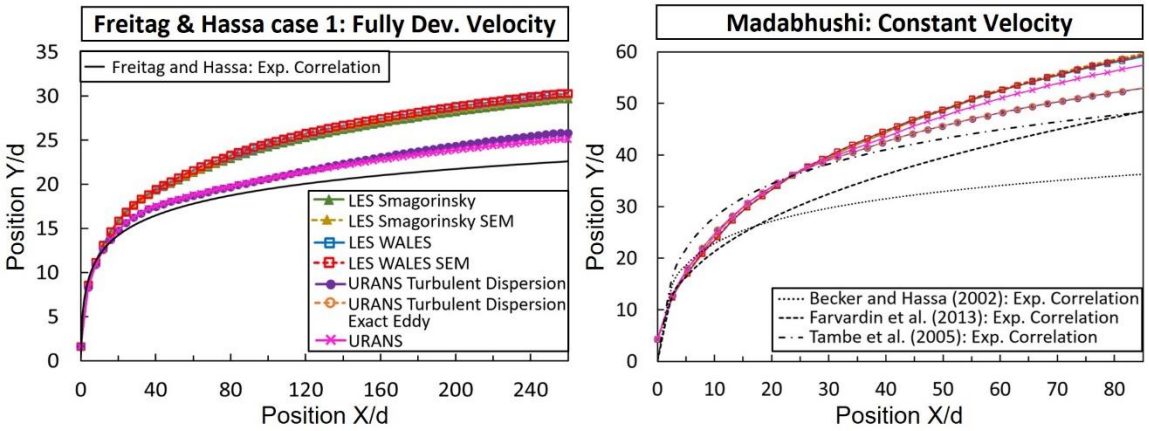

Figure 2: Maximum spray trajectory predicted by different turbulence approaches using the dataset from Freitag and Hassa (2008) case 1 and Madabhushi et al. (2004).

The local momentum flux ratio is expected to decrease from its imposed value presented in **Table 1** as the droplets travel through the domain and exchange their vertical momentum. **Figure 3** shows that all simulations captured the imposed value at the injection point (x=0), but only URANS with the datasets of Freitag and Hassa (2008) captured the expected axial evolution trend. Indeed, LES tends to predict that it increases in the near-field region until it reaches a peak value far superior to the one imposed. This is also the case for URANS with the datasets of Madabhushi et al. (2004), but the peak values remain significantly inferior to LES. Thus, URANS tends to capture more accurately the axial evolution trends of the local momentum flux ratio.

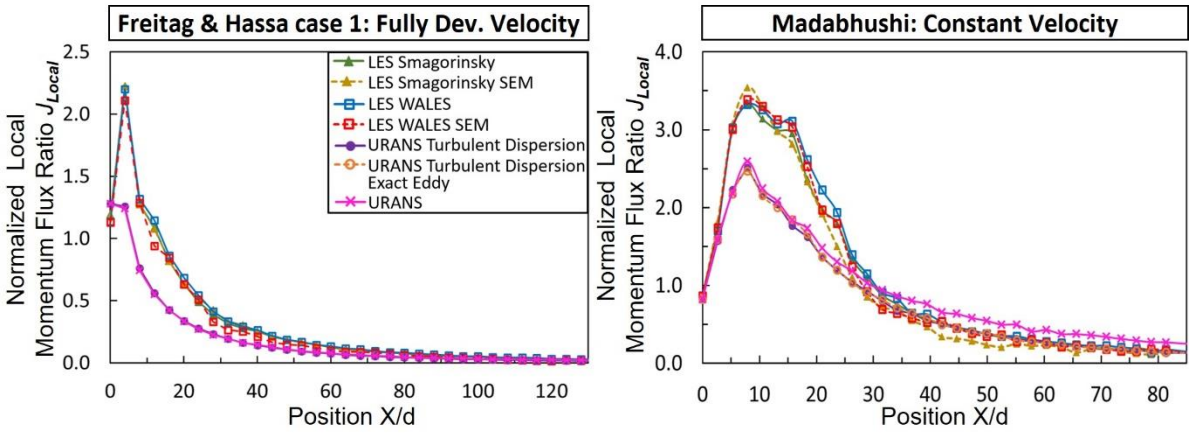

Figure 3: Normalized local Momentum flux ratio predicted by different turbulence approaches using the dataset from Freitag and Hassa (2008) case 1 and Madabhushi et al. (2004).

The higher jet trajectory predicted by LES is reflected by its significantly overpredicted local momentum flux ratio regardless of the conditions, especially in the near-field region as seen in **Figure 3**. In the near field region ($x/d \leq 30$), LES predicts J_{Local} on average higher by 35% and 72% for the dataset of Madabhushi et al. (2004) and Freitag and Hassa (2008) respectively. In addition, the higher relative difference with the latter agrees with the higher discrepancies observed in maximum spray trajectory compared to the

conditions of Madabhushi et al. (2008). This indicates that URANS might be sensitive to the boundary conditions.

For all simulations, the continuous phase velocity u drives the change in J_{Local} as its influence is more important compared to the vertical droplet velocity ($u_{pj}/u << 0.45$). Moreover, since u increases with the axial distance while u_{pj} decreases, its influence over the latter also increases axially. Thus, the higher momentum flux ratio locally predicted by LES results from its average underprediction of the axial gas velocity. Indeed, **Figure 4** shows that regardless of the condition, LES tends to predict a significantly lower gas velocity in the windward spray region, which is where the phases interaction is initially at its highest due to the jet penetrating the gas flow field.

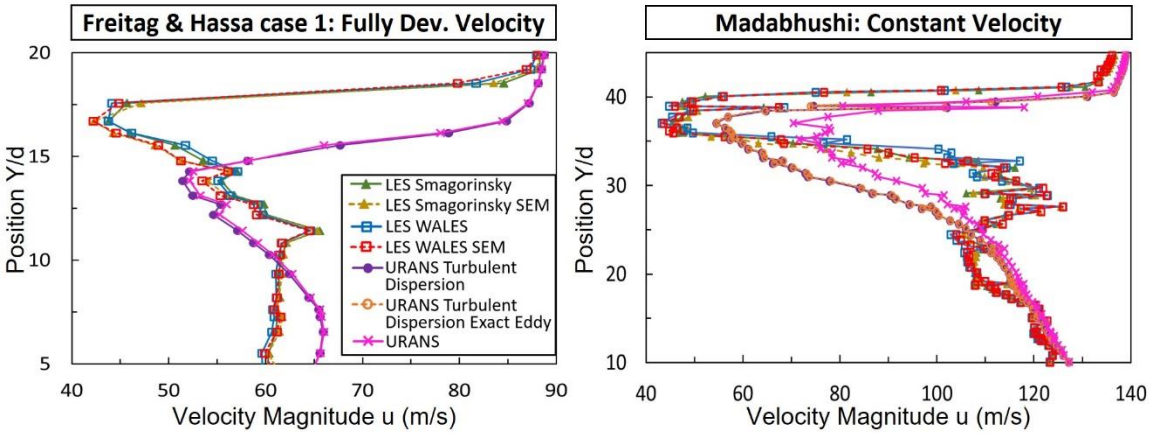

Figure 4: Centerline gas velocity profile at x/d=33 predicted by different turbulence approaches using the dataset from Freitag and Hassa (2008) case 1 and Madabhushi et al. (2004).

For liquid jets in crossflow, the vertical component of the droplet velocity dominates its axial component u_{pi} near the injection point ($u_{pj}/u_{pi} > 1$), which helps the jet penetrate the crossflowing gas flow field. LES predicts that the droplets conserve their vertical velocity on a longer axial distance ($x/d \leq 15$) for the higher jet velocity u_j conditions of Madabhushi et al. (2004), which enhances their vertical penetration. While the droplets exchange momentum with the continuous phase, u_{pi} increases and becomes more important than the vertical component ($u_{pj}/u_{pi} < 1$). Regardless of the conditions, LES tends to predict a reduced influence of u_{pi} especially in the near field region, which also facilitates the vertical penetration of the droplets. This is due to LES underpredicting the droplet axial velocity in the region where the phases interact most together. Indeed, it can be observed in **Figure 5** that LES predicts u_{pi} to decrease significantly in the spray core and windward region at transverse distances where URANS predicts the opposite.

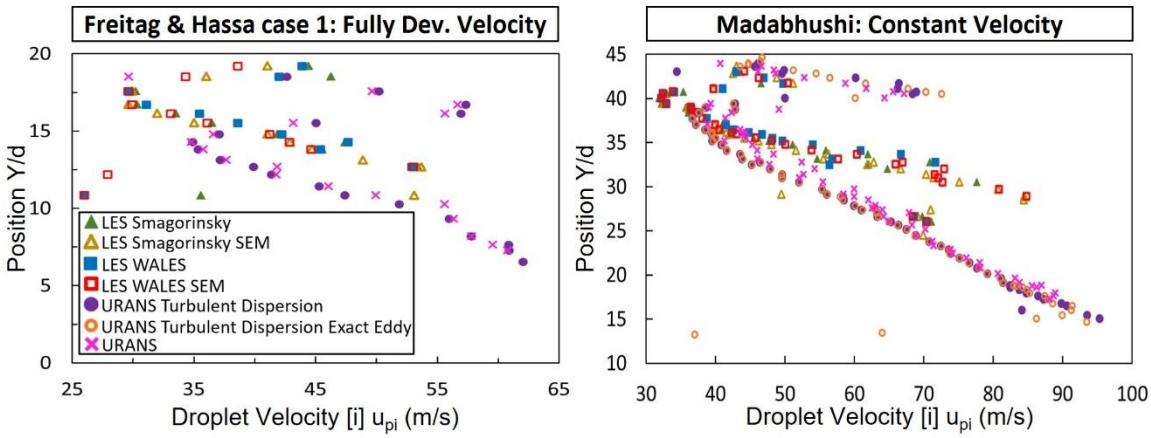

Figure 5: Centerline droplet axial velocity profile at x/d=33 predicted by different turbulence approaches using the dataset from Freitag and Hassa (2008) case 1 and Madabhushi et al. (2004).

4.1.2 URANS VS LES: SMD PREDICTIONS

Regardless of the experimental conditions, **Figure 6** shows that LES tends to predict a smaller SMD than URANS in the leeward and spray core regions because of its local overprediction of the continuous phase velocity presented in **Figure 4**. This is due to the flow field adapting itself to compensate for the significant decrease in velocity occurring at the higher transverse distance. Although this causes the local particle axial velocity to also increase as shown in **Figure 5**, the change is not as important. Thus, LES tends to predict a higher particle slip velocity in the leeward and spray core regions, which locally enhance the breakup process and reduces the SMD.

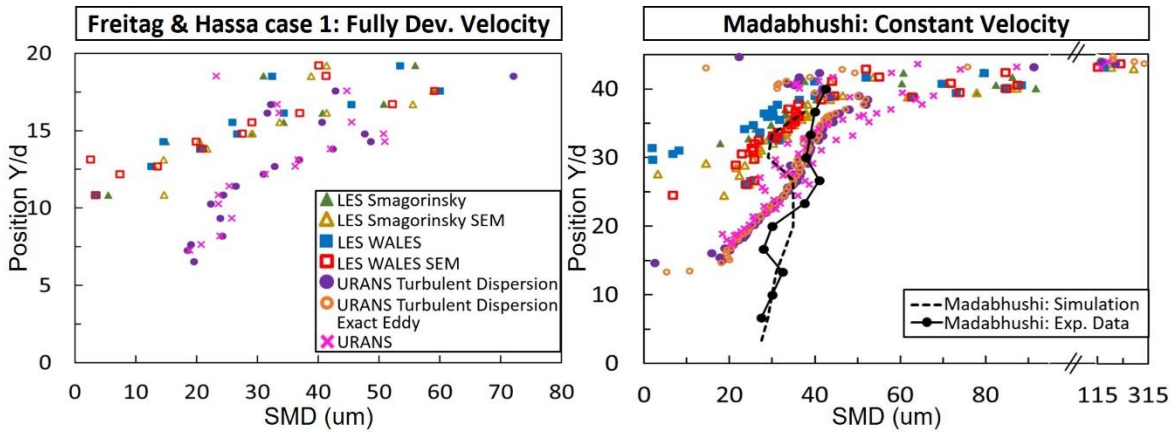

Figure 6: Centerline SMD at x/d=33 predicted by different turbulence approaches using the dataset from Freitag and Hassa (2008) case 1 and Madabhushi et al. (2004). *

In addition, LES tends to predict a higher SMD in the windward region due its local underprediction of the continuous phase velocity. This causes the droplet axial velocity to decrease to values close to those of the gas velocity. As a result, LES tends to predict a locally lower slip velocity that reduces the breakup process, hence the higher SMD observed.

Regarding the accuracy of the predictions, it is possible to observe that LES and URANS tend to underpredict the SMD in the leeward region compared to the data from Madabhushi et al. (2004). LES also tends to underpredict it in the spray core region, which agrees with what has been reported in the literature regarding the SSD model (Apte et al., 2003; Apte et al., 2009; Gorokhovski et al., 2012). However, the current methodology combined with the URANS turbulence approach achieves better agreement with the data in the spray core region as the average error is less than 4%. Moreover, as the transverse distance increases, the Madabhushi breakup model underpredicts the SMD which agrees with the current LES predictions. Further studies should be done on the effect of coupling a collision and coalescence model with the presented numerical methodology to improve the SMD predictions in the wake region behind the jet.

The current numerical methodology also tends to predict a higher maximum and minimum droplet transverse location compared to the experimental data of Madabhushi et al. (2004). This agrees with the previously described overpredicted maximum trajectory compared to the experimental correlation from Freitag and Hassa (2008). Thus, it possible to conclude that the SSD breakup model tends to overpredict the spray trajectory and underpredict the vertical dispersion for jets in crossflow. This could be due to an overall underestimation of the aerodynamics effects on the jet column bending, the turbulent interactions or the momentum transfer. Considering that most of these processes occur in the near-field region, future

* "Madabhushi: Exp. Data" and "Madabhushi: Simulation" curves/data points used with permission of ASME, from *Simulation of the Break-Up of a Liquid Jet in Crossflow at Atmospheric Conditions, Madabhushi, R.K., Leong, M.Y. and Hautman, D.J., vol. 1, pp. 697–704, 2004.*; permission conveyed through Copyright Clearance Center, Inc.

work should be done to study the effect of coupling the current approach with a locally higher fidelity model for turbulent jets in crossflow.

4.1.3 URANS VS LES: EFFECT OF MOMENTUM EXCHANGE ON PREDICTIONS

As previously discussed, the higher jet trajectory and lower SMD predicted by LES are both related to lower velocity predictions. Regardless of the conditions, LES underpredicts the droplet axial velocity because it tends to predict a lower net exchange of axial momentum as seen in **Figure 7**. Thus, the droplets receive less axial momentum from the continuous phase, which could be caused by the locally lower axial velocity of the latter compared to URANS, as shown in **Figure 4.**

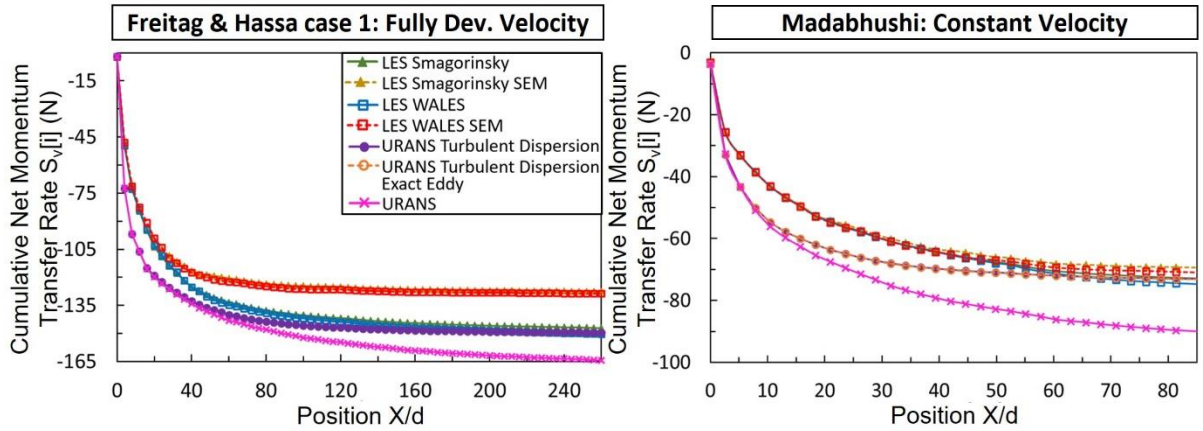

Figure 7: Cumulative net transfer rate of axial momentum predicted by different turbulence approaches using the dataset from Freitag and Hassa (2008) case 1 and Madabhushi et al. (2004).

Figure 8 shows that LES also tends to underpredict the net exchange of vertical momentum $S_v[j]$ transferred from the droplets to the continuous phase. This explains why LES tends to predict that they conserve their vertical velocity component on a longer axial distance. For the conditions of Freitag and Hassa (2008), this causes LES to overpredict u_{pj}, which contributes to enhance its local momentum flux ratio and maintain it higher than the one predicted by URANS along the domain.

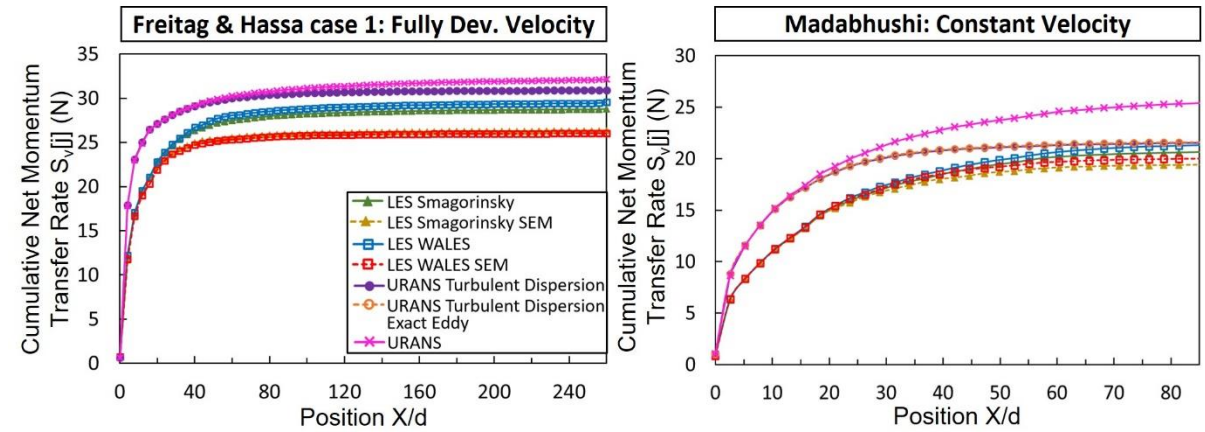

Figure 8: Cumulative net transfer rate of vertical momentum predicted by different turbulence approaches using the dataset from Freitag and Hassa (2008) case 1 and Madabhushi et al. (2004).

It is also possible to observe that the total net momentum transfer for URANS and LES mostly occurs in the near-field region as 80% of it is exchanged before x/d=30. Afterwards, the exchange of axial momentum is mostly governed by the turbulent characteristics of the flow field. Thus, it is possible that LES tends to underpredict the net exchange of axial momentum because of an underprediction of the turbulent

interactions. The continuous phase would then have less axial momentum to transfer due to its resulting lower axial velocity, as previously shown in **Figure 4.**

4.1.4 URANS VS LES: EFFECT OF TURBULENT INTERACTIONS ON PREDICTIONS

Regardless of the experimental conditions, LES tends to predict significantly smaller turbulent interaction times across the entire spray as seen in **Figure 9**. In the near-field region, they are in the same order of magnitude as URANS up to x/d=10 and x/d=30 for the conditions of Freitag and Hassa (2008) and Madabhushi et al. (2004) respectively. As previously discussed, there are no significant differences in maximum spray trajectories in these regions. As the droplets travel through the turbulent flow field, URANS predicts that the turbulent interactions increase as expected. This is not the case for LES as there are no comparable changes in τ_I. As a result, LES tends to predict τ_I values multiple order of magnitude lower than URANS. Thus, it is possible to conclude that the maximum spray trajectory increases when the turbulent interactions decrease as it allows the droplets to further penetrate the turbulent flow field downstream of the injection point.

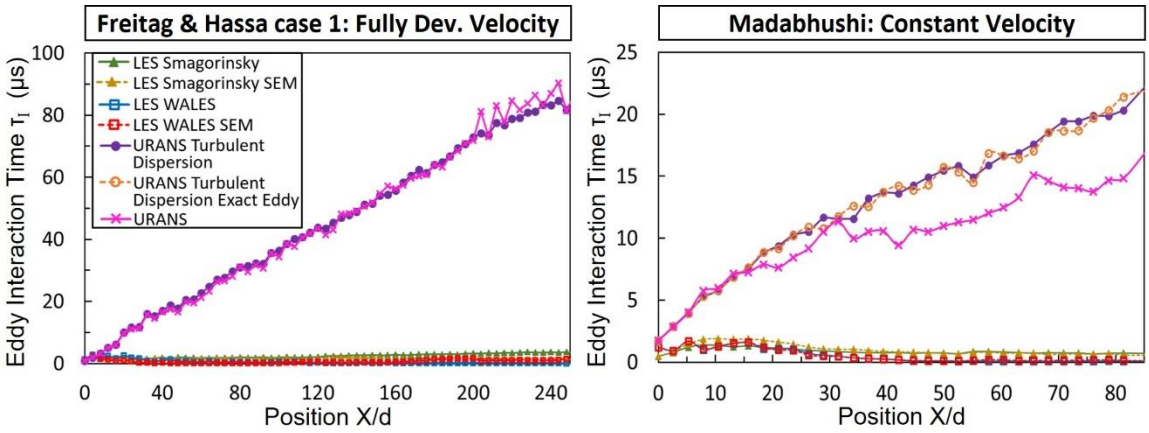

Figure 9: Eddy Interaction Time predicted by different turbulence modeling approaches using the dataset from Freitag and Hassa (2008) case 1 and Madabhushi et al. (2004).

The lower turbulent interactions predicted by LES could also be facilitating the radial dispersion of the droplets. This might explain why the spray width tends to be larger on average by 19% and 226% compared to URANS for the conditions of Madabhushi et al. (2004) and Freitag and Hassa (2008) respectively. The higher relative difference for the latter further supports the previous observations regarding the sensitivity of the URANS approach to the boundary conditions.

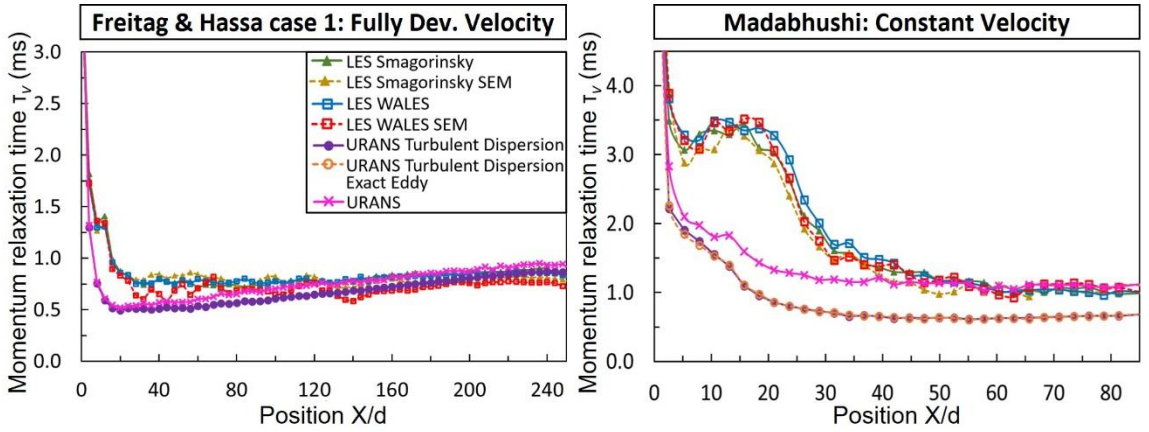

Figure 10: Momentum relaxation time predicted by different turbulence approaches using the dataset from Freitag and Hassa (2008) case 1 and Madabhushi et al. (2004).

For all the simulations, the turbulent interactions are predicted to be governed by the eddy transit time τ_c. This means that the droplets are predicted to have a slip velocity strong enough to pass through the turbulent eddies (Gosman and Ioannides, 1981). As presented in Eq.(22), τ_c decreases with a decreasing eddy length scale and with an increasing momentum relaxation time and particle slip velocity. As seen in **Figure 10**, LES tends to predict a higher momentum relaxation time in the primary breakup region, but no significant differences are predicted in the far-field region. Regarding the average particle slip velocity, although LES tends to predict it higher by 8% compared to URANS in the secondary breakup region for the dataset of Madabhushi et al. (2004), it predicts it lower by 13% in the near-field region. Moreover, there are no significant differences predicted in u_s for the dataset of Freitag and Hassa (2008) in the far-field region and LES also tends to predict it lower by 15% in the near-field region. Thus, the lower eddy length scale predicted by LES is likely the main factor behind its lower eddy transit time, as shown in **Figure 11**. This is even more plausible considering that l_e is also underpredicted by multiple order of magnitudes except in the primary breakup region, similarly to τ_I.

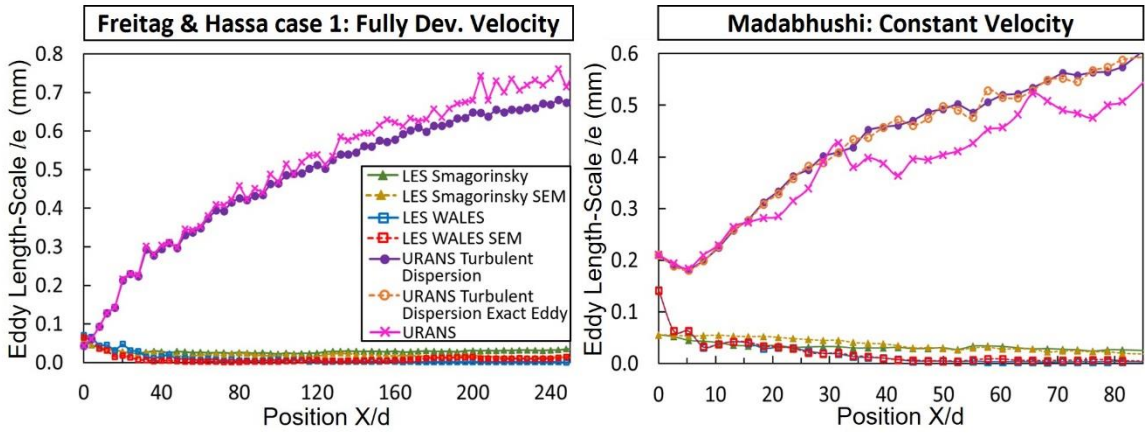

Figure 11: Eddy Length-scale predicted by different turbulence approaches using the dataset from Freitag and Hassa (2008) case 1 and Madabhushi et al. (2004).

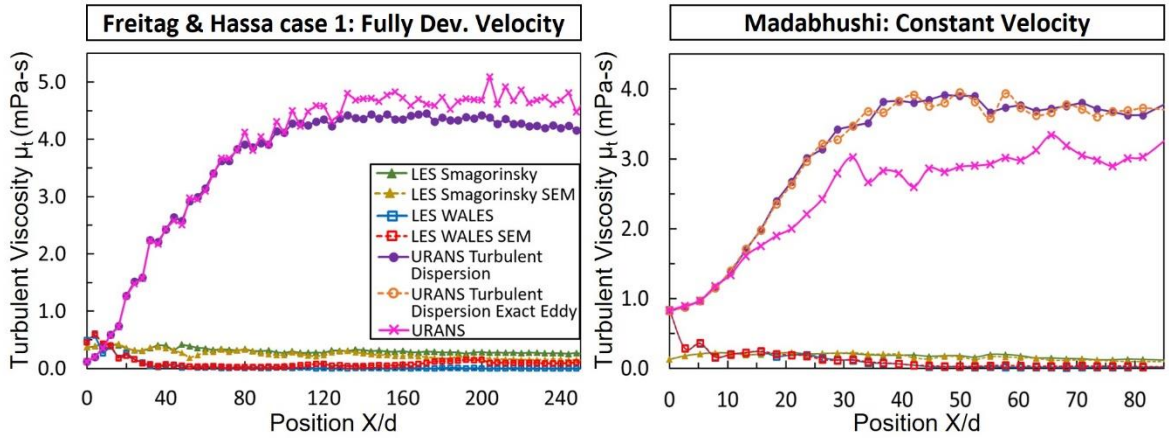

Figure 12: Turbulent viscosity predicted by different turbulence approaches using the dataset from Freitag and Hassa (2008) case 1 and Madabhushi et al. (2004).

As presented in Eq.(23), the eddy length scale decreases proportionally with the turbulent viscosity and for an increasing turbulent kinetic energy. For the conditions of Freitag and Hassa (2008), the latter predicted by LES contributes to reducing l_e as it is on average almost 2.5 times the values predicted by URANS. However, it's the opposite for the conditions of Madabhushi et al. (2004) as LES tends to predict the turbulent kinetic energy smaller by 23% on average. As seen in **Figure 12**, regardless of the conditions, LES tends to predict a significantly smaller μ_t values, especially in the secondary breakup region as it

becomes multiple order of magnitude lower than URANS. Indeed, LES predicts μ_t to be on average smaller by 83% and 91% compared to URANS for the conditions of Freitag and Hassa (2008) and Madabhushi et al. (2004) respectively. Moreover, URANS is able to capture the expected axial evolution of μ_t as it increases until its value stabilizes with the turbulent length scale. Therefore, it is possible to conclude that the lower turbulent viscosity field that LES tends to predict may result in less turbulent kinetic energy being transferred to the discrete phaseF, allowing the droplets to penetrate further into the domain. This would also explain the trends observed in SMD predictions. Moreover, the lower axial velocity of the continuous phase predicted by LES could be due to an underprediction of the filtered stress tensor applied to its filtered momentum and energy transport equations since it's proportional to μ_t.

The LES approach resolves directly on the numerical grid the turbulent large-scale motions and accounts for the effects of the subgrid-scale motions on the large scale through a SGS model (Wang and Squires, 1996; Yang et al., 2008). The filtering of the small scales means that the effects of the associated velocity fluctuations are not accounted for in the computation of the continuous phase velocity (Yang et al., 2008; Johnson and Meneveau, 2017; Gorokhovski and Oruganti, 2021). The LES approach alone can be considered sufficient to capture the turbulent dispersion if the portion caused by the unresolved smaller-scale motions is negligible (Ničeno et al., 2008). However, this does not apply when the local flow conditions of the physical processes modelled are strongly influenced by the velocity gradient tensor or when large Reynolds numbers are used, such as with turbulent liquid jets (Wang and Squires, 1996; Yang et al., 2008; Johnson and Meneveau, 2017 ; Gorokhovski and Oruganti, 2021). In fact, neglecting the contribution of the unresolved velocity field when using LES with the Lagrangian approach has been reported to underpredict the droplet turbulent dispersion (Wang and Squires, 1996; Yang et al., 2008; Johnson and Meneveau, 2017). Thus, the conclusions of the present study regarding LES agree with what has been reported in the literature for coflowing sprays. Indeed, other studies have also observed that it results in lower exchange rates between the phases, an overprediction of the liquid penetration length, a smaller gas entrainment and an overall increase in discrepancies with the experimental data (Wang and Squires, 1996; Jangi,et al, 2015; Tsang and Rutland, 2017). To improve the accuracy of the predictions of the LES approach for turbulent liquid jets in high-speed crossflow, additional modelling is recommended to account for the subgrid scale Lagrangian velocity field as suggested by other studies conducted for coflowing sprays (Wang and Squires, 1996; Yang et al., 2008; Johnson and Meneveau, 2017).

4.2 LES: EFFECT OF SGS AND SEM

It is possible to observe in the previous section that the SGS models and SEM predict similar droplet and gas velocities, SMD and spray trajectory regardless of the conditions. This is due to their similar predictions of turbulent interactions and net exchange of momentum. However, for the dataset of Freitag and Hassa (2008), although the spray width predicted using both SGS models also tend to agree together when coupled with the SEM, using the latter results in a 31% increase. This indicates that the effect of the SEM on the spray characteristics is sensitive to the conditions.

4.3 URANS: EFFECT OF TURBULENT DISPERSION MODEL

The effect of the turbulent dispersion model is assessed by comparing the URANS predictions with and without it, which are included in the Figures of section 4.1. For the conditions of Freitag and Hassa (2008), it does not have a significant impact on most spray characteristics as it predicts a similar droplet and gas velocity, SMD and spray trajectory. This is due to its unsignificant impact on the net exchange of momentum and turbulent interactions**.**

For the low pressure and high moment flux ratio conditions of Madabhushi et al. (2004), the turbulent dispersion model has a significant impact on the spray characteristics predicted in the far-field region. As seen in **Figure 2**, it locally reduces the overpredicted spray trajectory by at least 8% due to a 28% average decrease in local momentum flux ratio. As seen in **Figure 7** and **Figure 8**, using the turbulent dispersion model increases the rate at which the total net momentum is exchanged since 80% of it occurs before x/d=15. This indicates that the particles transfer most of their vertical momentum to the continuous phase

earlier in the domain. This is illustrated in **Figure 13** by the higher gas vertical velocity u[j] predicted when using the turbulent dispersion model. Thus, u_{pj} tends to be smaller in the secondary breakup region and leads to lower J_{Local}.

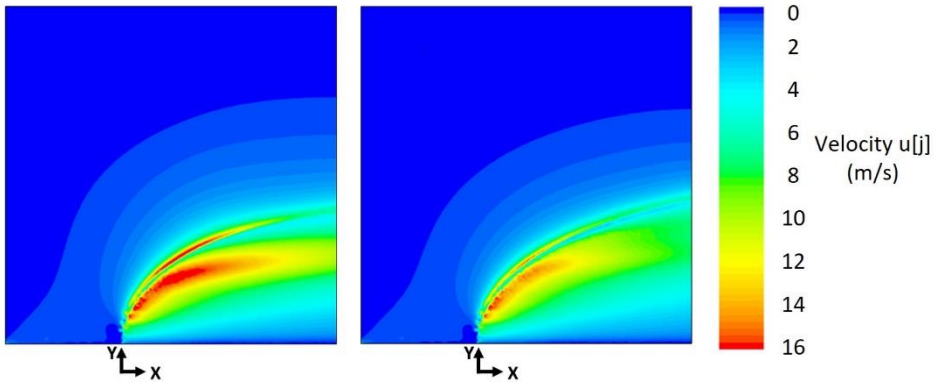

Figure 13: Continuous phase vertical velocity predicted by URANS with [left] and without [right] the turbulent dispersion model using the dataset from Madabhushi et al. (2004).

The differences in spray characteristics observed in the secondary breakup region for the conditions of Madabhushi et al. (2004) can be attributed to the lower turbulent interactions predicted when the turbulent dispersion is not accounted for. Indeed, **Figure 9** shows that it results on average in a 21% decrease in turbulent interaction time above x/d=15. This can be attributed to the local 20% average decrease in turbulent viscosity shown in **Figure 12**. Like for LES, the lower turbulent interactions predicted without the turbulent dispersion model locally increase the discrepancies in spray trajectory compared to the experimental data. Considering that this does not occur for the conditions of Freitag and Hassa (2008), not accounting for the turbulent dispersion might cause the URANS turbulence approach to be more sensitive to the boundary conditions.

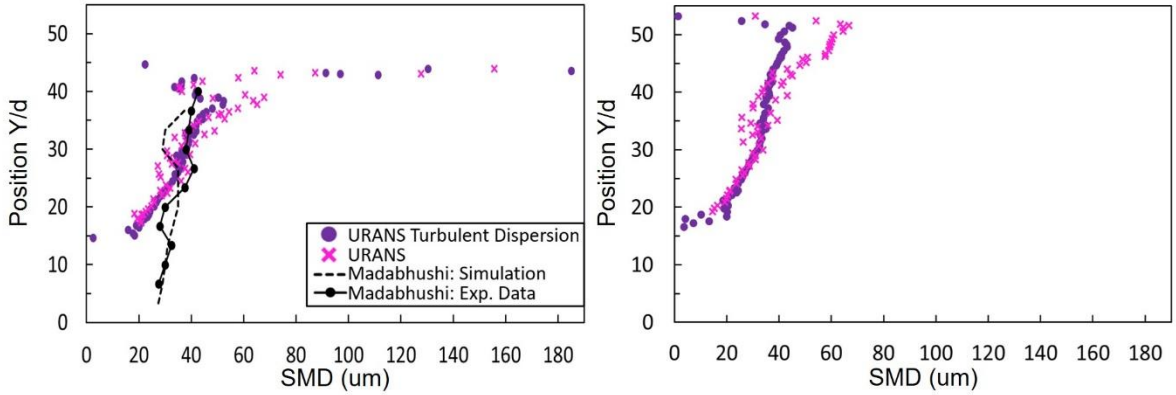

Figure 14: Centerline SMD at x/d=33 [right] and x/d=66 [left] predicted by URANS with and without the turbulent dispersion model using the dataset from Madabhushi et al. (2004).**

Regardless of the conditions, the turbulent dispersion model does not have a significant impact on the SMD in the leeward and spray core region as seen in **Figure 6.** The underprediction of the SMD in the leeward region agrees with what has been reported by other URANS numerical studies conducted on the SSD model (Nihasigaye and al., 2021). However, using the turbulent dispersion model for the conditions of Madabhushi et al. (2004) tends to improve the accuracy in the windward region as it reduces the SMD. For all the simulations conducted, the SMD increases with the transverse distance, which indicates that the

** "Madabhushi: Exp. Data" and "Madabhushi: Simulation" curves/data points used with permission of ASME, from *Simulation of the Break-Up of a Liquid Jet in Crossflow at Atmospheric Conditions, Madabhushi, R.K., Leong, M.Y. and Hautman, D.J., vol. 1, pp. 697–704, 2004.*; permission conveyed through Copyright Clearance Center, Inc.

breakup process is concentrated in the leeward and spray core region. As the droplets travel through the domain, the SMD tends to change less in those regions due to their sizes no longer meeting the critical radius r_c required for breakup imposed by the SSD model. Thus, the secondary breakup process is predicted to mostly occur in the windward region. Because the rate of momentum exchange in the secondary breakup region decreases significantly without the turbulent dispersion model, the breakup process in the windward region takes a longer axial distance to be completed. Indeed, **Figure 14** shows that the discrepancies in the windward region increase with the axial distance due to the SMD still being significantly overpredicted without the turbulent dispersion model.

Regardless of the conditions, using the turbulent dispersion model increases the spray width. For the high-pressure conditions of Freitag and Hassa (2008), it enhances the radial diffusion to levels comparable to LES without the SEM. For the lower pressure of Madabhushi et al. (2004), it predicts the largest spray width as it increases on average by 45% compared to LES. Additional experimental studies on the radial diffusion of turbulent jets in crossflow at high pressures and momentum flux ratios are needed to evaluate the accuracy of the spray widths predicted.

The effect limiting the parcel time-step δt_p to sum up to the exact eddy interaction time when using the turbulent dispersion model was assessed with the dataset from Madabhushi et al. (2004). As shown in **Figure 7** to **Figure 9**, it does not have any significant impact on the net exchange of momentum or turbulent interactions. This explains why no significant differences could be observed in terms of droplet and gas velocities, SMD, spray trajectory and width. This indicates that the strategy used to limit δt_p allows to capture the turbulent interactions that affect the spray characteristics the most. Considering the higher computational cost of using the exact eddy interaction time sub-model, it is recommended to estimate the Lagrangian courant numbers with the strategy described in Section 3.3 and to impose a Co_{min} value as small as possible.

4.4 VELOCITY PROFILE SENSITIVITY: LES

The sensitivity of the LES approach to the inlet velocity profile was assessed using case 1 from Freitag and Hassa (2008) with a constant velocity profile. It is possible to conclude from **Figure 15** that the tendency of LES to overpredict the spray trajectory is independent of the velocity profile. Indeed, using a constant velocity profile increases the average relative error to 33%.

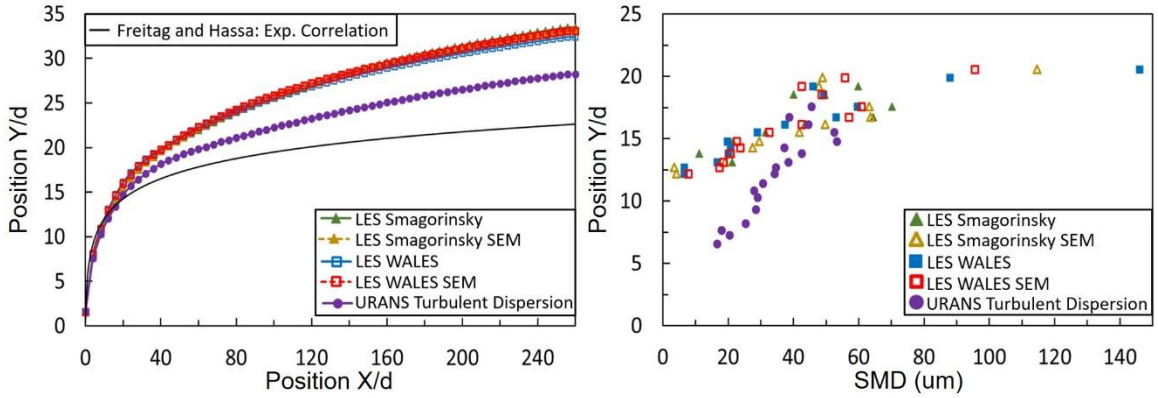

Figure 15: Maximum spray trajectory and centerline SMD at x/d=33 predicted by different turbulence approaches using case1 from Freitag and Hassa (2008) for a constant velocity profile**.**

The tendency of LES to predict a lower SMD in the spray leeward and core regions is also independent of the velocity profile. This is also true for the local SMD values predicted. However, LES tends to predict a significant increase in SMD at the highest transverse distance when using a constant velocity profile. This agrees with the predictions made by URANS and LES for the conditions of Madabhushi et al. (2004) as seen in **Figure 6.** Considering they both use a constant velocity profile, it could indicate that the accuracy

of the near-field region breakup process predicted by LES at the highest interphase is more sensitive to changes in the local velocity field.

These results can be explained by the same factors previously described for the dataset of Madabhushi et al. (2004) and Freitag and Hassa (2008) with a fully developed velocity profile. Indeed, the eddy interaction time and total net transfer rate of momentum across the entire spray predicted by LES are also lower, on average by 84% and 16% respectively compared to URANS with the turbulent dispersion model. Thus, it can be concluded that LES tends to underpredict these important parameters of the phase interactions regardless of the velocity profile.

It is also possible to conclude that regardless of the velocity profile, the SEM and the SGS model do not have a significant impact on the spray characteristics, except for the spray width at the higher-pressure conditions of Freitag and Hassa (2008). Indeed, the SEM tends to predict a larger spray width that agree together regardless of the velocity profile. Moreover, using a constant velocity profile tend to increase the spray width predicted except for the Smagorinsky SGS model used without the SEM where the opposite occurs. As a result, the latter tends to predict a spray width on average 41% smaller than the WALES SGS model. Thus, the spray width predicted without the SEM do not agree together when using a constant velocity profile. This indicates that the radial dispersion predicted by the Smagorinsky SGS model might be sensitive to the continuous velocity field for turbulent jets in crossflows, which corroborates previous findings available in the literature for coflowing sprays (Apte et al., 2003; Apte et al., 2009).

4.5 VELOCITY PROFILE SENSITIVITY: URANS

The sensitivity of the URANS turbulence approach to the inlet velocity profile was only studied with the turbulent dispersion model as it showed the best agreement with the data as discussed in Section 4.3. Regardless of the conditions or turbulence approach, assuming a constant velocity profile tends to increase the spray jet trajectory. Indeed, the error with the experimental data from Freitag and Hassa (2008) in the far-field region increases to 25% as seen in **Figure 15.** The difference is less significant for the dataset from Madabhushi et al. (2004) as it only increases the trajectory by a maximum of 4%. This indicates that the numerical approach might be less sensitive to higher jet velocities if the gas velocity is also high. Therefore, it can be concluded that the dispersed phase is sensitive to small changes in the gas velocity field regardless of the turbulence approach, but the importance of the resulting discrepancies might depend on the boundary conditions. These results emphasise the importance of accounting for the gas velocity profile.

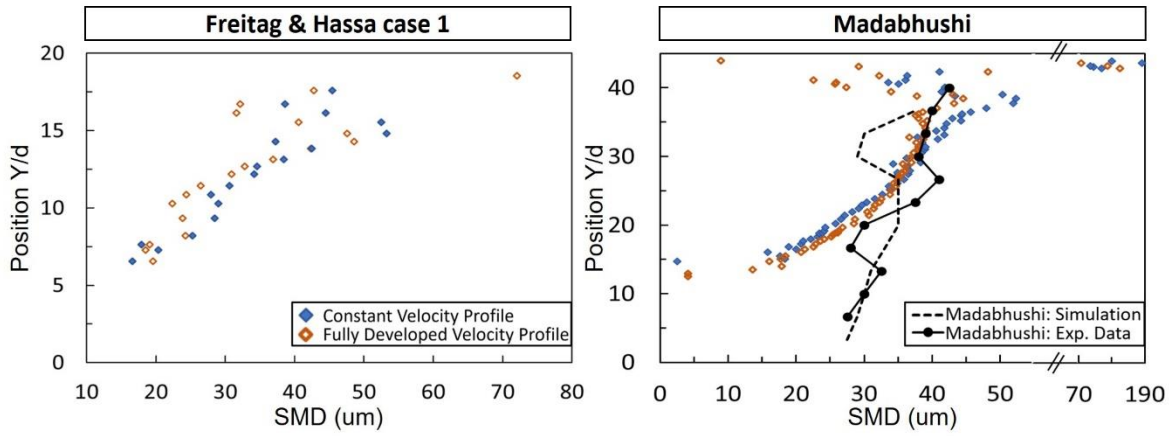

Figure 16: Centerline SMD at x/d=33 predicted with the turbulent dispersion model obtained using the dataset from Freitag and Hassa (2008) case 1 and Madabhushi et al. (2004).***

*** "Madabhushi: Exp. Data" and "Madabhushi: Simulation" curves/data points used with permission of ASME, from *Simulation of the Break-Up of a Liquid Jet in Crossflow at Atmospheric Conditions, Madabhushi, R.K., Leong, M.Y. and Hautman, D.J., vol. 1, pp. 697–704, 2004.*; permission conveyed through Copyright Clearance Center, Inc.

Regardless of the conditions or turbulence approach, using a constant velocity profile tends to increase the SMD predicted in the windward region as seen in **Figure 16**. This is due to the higher gas velocity field that the droplets in the windward region are subjected to when using a fully developed velocity profile. Indeed, this results in a higher u_s which locally enhances the breakup process. For the conditions of Freitag and Hassa (2008), this effect can also be observed in the leeward and spray core regions. Thus, the sensitivity of the SMD to the velocity profile might also depend on the boundary conditions. This aspect is further studied in section 4.6. Further studies could be done to improve the SMD predictions by coupling some aspects of the SSD model, such as the particle-size distribution, with the Madabhushi breakup model, which uses a root-normal distribution dependant on the parent droplet size (Madabhushi et al., 2004).

4.6 BOUNDARY CONDITIONS SENSITIVITY: URANS

The sensitivity of the numerical methodology developed to the boundary conditions was further assessed with both velocity profiles using the datasets from Freitag and Hassa (2008). This study was limited to the turbulent dispersion model for the same reasons stated in section 4.5. Regardless of the velocity profile, increasing the pressure does not tend to have a significant impact on the predictions as seen in **Figure 17.** Indeed, increasing P_g from 4 to 8 bar with a constant J of 6 causes a 3% absolute decrease in the relative error with the experimental data for both velocity profiles. Thus, the lower discrepancies observed previously with the dataset of Madabhushi et al. (2004) are more likely caused by its higher momentum flux ratio.

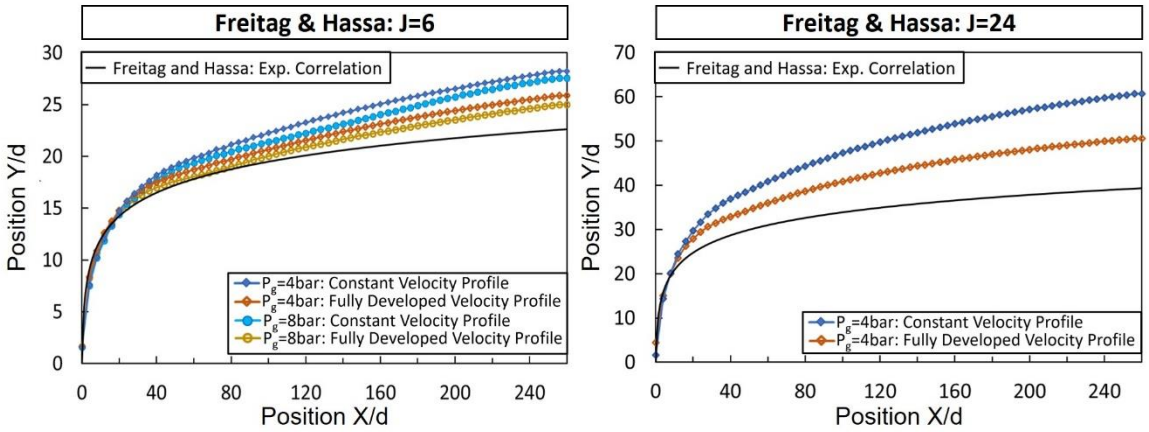

Figure 17: Maximum trajectory predicted with the turbulent dispersion model obtained for constant and fully developed velocity profile using the datasets from Freitag and Hassa (2008).

Moreover, the slightly lower trajectories predicted at the higher-pressure conditions indicate that the numerical methodology accounts for the pressure effects on the spray characteristics. Although some experimental correlations for jets in crossflow at standard temperature and high-pressure consider the trajectory to be independent of P_g (Freitag and Hassa, 2008; Ragucci et al., 2007), others consider that it decreases with an increasing pressure (Elshamy and Jeng, 2005; Song et al., 2014). The ability of the numerical methodology to capture the pressure effects was expected since the SSD model has been validated for pressures up to 50 bar although for coflowing gas (Apte et al., 2003; Apte et al., 2009). Thus, the present work suggests that the SSD model is also suitable for predicting the trajectory of jets in crossflow under high pressure conditions up to 8 bar.

Regardless of the velocity profile, the numerical methodology tends to be sensitive to higher jet velocities. Indeed, increasing J from 6 to 24 with a constant P_g of 4 bar causes the average relative error to increase from 8% to 21% and from 16% to 40% with a fully developed and constant velocity profile respectively. However, this does not indicate that the numerical methodology studied is not suitable for high momentum flux ratios. In fact, the momentum flux ratios from the datasets of Freitag and Hassa (2008) are lower than the one from Madabhushi et al. (2004) as shown in **Table 1**. Despite this, the SMD predicted tends to agree

well with the data and the jet trajectory is less sensitive to local changes in velocity. The main difference between both datasets lies in the imposed jet to gas velocity ratio, which is significantly lower for Madabhushi et al. (2004) ($u_j/u_g \approx 0.22$) compared to the highest momentum flux ratio condition (case 2) from Freitag and Hassa (2008) ($u_j/u_g \approx 0.37$) as seen in **Table 1**. A higher u_j/u_g ratio indicates that the droplets conserve their vertical momentum on a longer axial distance, which enhances their ability to penetrate the continuous phase due to the resulting higher droplet velocity ratio u_{pj}/u_{pi}.

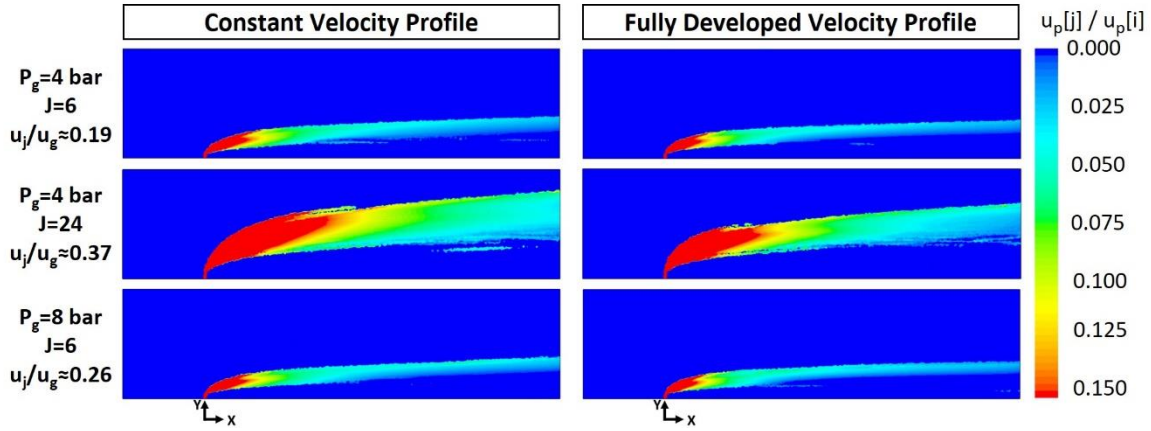

Figure 18: Droplet velocity ratio predicted with the turbulent dispersion model obtained using the datasets from Freitag and Hassa (2008) case 1 [top], case 2 [middle], case 3 [low].

Figure 18 shows that the discrepancies in spray trajectory with the experimental correlation tend to increase with the imposed u_j/u_g ratio. Indeed, case 2 has the highest u_j/u_g ratio imposed and highest relative error, followed by case 1. The behaviour of case 3 indicates that high-pressure conditions reduce the sensitivity to the imposed u_j/u_g ratio. Moreover, for a given u_j/u_g ratio, the droplet velocity ratio remains high on a longer axial distance with a constant velocity profile which reduces the accuracy. Thus, the numerical methodology seems to be more sensitive to the imposed jet to gas velocity ratio than to the momentum flux ratio. This corroborates the findings of Nihasigaye et al. (2021) that the predictive capabilities of the SSD model with the URANS approach tend to be sensitive to an increase in maximum droplet velocity. Future work should be done to reduce the sensitivity of the SSD model's predictive capabilities to the imposed velocities.

5. CONCLUSION

In summary, an unsteady numerical methodology using the SSD breakup model combined with TAB distortion model was validated and the effect of different turbulence approaches were assessed for turbulent liquid fuel jets in high-speed crossflow. Good agreement with the experimental data was achieved with URANS for the SMD and spray trajectory at standard and high pressures over a wide range of momentum flux ratios and gas Weber numbers. Coupling the methodology with the turbulent dispersion model is recommended as it was shown to improve the predictions regardless of the conditions or inlet velocity profile. The strategy used to determine the values of the Lagrangian courant numbers is also recommended as it captures the turbulent interactions to a level similar to the Exact Eddy Time sub-model, but at a lower computational cost. To improve the predictions, future work should be done on coupling the SSD model with higher fidelity models in the primary breakup region.

Regardless of the experimental conditions or inlet velocity profile, LES used with the standard subgrid scale models tend to predict higher discrepancies with the experimental data. Indeed, it was shown to overpredict significantly the spray trajectory as well as underpredict the SMD in the leeward and spray core regions. This might be caused by its tendency to predict a lower turbulent viscosity field, which results in lower turbulent interactions and lower momentum exchanges. In addition, the Synthetic Eddy Method is not deemed worth the extra computational cost due to its unsignificant impact on the predictions. The present study recommends using the WALES SGS model over the Smagorinsky SGS model since the latter was

shown to be more sensitive to local changes in the velocity field. However, in order to use LES as a robust numerical tool to hasten the delivery of new sustainable technologies, its coupling with the Lagrangian approach needs to be improved. Future work should be done on assessing the impact of coupling LES with a stochastic turbulent dispersion model and of using a SGS model that accounts for the droplets sub-filtered acceleration as described in Gorokhovski and Oruganti (2021) and references therein.

This study also concludes that regardless of the turbulence approach used, proper consideration of the upstream gas velocity profile is essential to accurately predict the spray characteristics for turbulent jets in crossflow. This is especially important when trying to validate and calibrate numerical models as the predictions were shown to be sensitive to changes in the velocity field.

6. ACKNOWLEDGMENTS

This study is based on a PhD research project supported by Siemens Energy and Cranfield University. The financial support provided by the Canadian Centennial Scholarship Fund (CCSF) and the Natural Sciences and Engineering Research Council of Canada (NSERC) is gratefully acknowledged.

7. REFERENCES

Amighi, A., Liquid jets in crossflow at elevated temperatures and pressures, *PhD*, University of Toronto, 2015.

Amsden, A.A., Ramshaw, J.D., O'Rourke, P.J. and Dukowicz, J.K., KIVA: A Computer Program for Two- and Three-Dimensional Fluid Flows with Chemical Reactions and Fuel Sprays, *Los Alamos National Labs*, United-States, Rept LA-10245-MS, 1985.

Apte, S.V., Gorokhovski, M. and Moin, P., LES of atomizing spray with stochastic modeling of secondary breakup, *International Journal of Multiphase Flow*, vol. 29, pp. 1503–1522, 2003. DOI:10.1016/S0301-9322(03)00111-3

Apte, S.V., Mahesh, K., Gorokhovski, M. and Moin, P., Stochastic modeling of atomizing spray in a complex swirl injector using large eddy simulation. *Combustion Institute*, vol. 32, pp. 2257–2266, 2009. DOI: 10.1016/j.proci.2008.06.156

Baumgarten, C. Mixture formation in internal combustion engines, Heat and mass transfer. Berlin; *Springer*, pp. 85-210, 2006.

Beale, J. C. and Reitz, R. D., Modeling spray atomization with the KHRT hybrid model, *Atomization and Sprays*, vol. 9, no.6, pp. 623–650, 1999. DOI: 10.1615/AtomizSpr.v9.i6.40

Becker, J. and Hassa, C. Breakup and atomization of a kerosene jet in crossflow at elevated pressure, *Atomization and Sprays*, vol. 12, nos. 1-3, pp. 49-67, 2002. DOI: 10.1615/AtomizSpr.v12.i123.30

Behzad, M., Ashgriz, N. and Karney, B.W., Surface breakup of a non-turbulent liquid jet injected into a high-pressure gaseous crossflow. *International Journal of Multiphase Flow*, vol. 80, pp. 100–117, 2016. DOI: 10.1016/j.ijmultiphaseflow.2015.11.007

Bellofiore, A., Cavaliere and A., Ragucci, R., Air density effect on the atomization of liquid jets in crossflow, *Combustion Science and Technology*, vol. 179, nos. 1-2, pp. 319-342, 2005. DOI: 10.1080/00102200600809563.

Blanchard, R., and Shi, S., Validation of a stochastic droplet breakup model applied to a liquid jet in turbulent crossflow. *AFM 2012*, Split, Croatia, pp. 371–378, 2012. DOI: 10.2495/AFM120331

Bravo, L.G., Kim, D., Ham, F. and Kerner, K.A., High Fidelity Simulations of Primary Breakup and Vaporization of Liquid Jet in Cross Flow (JICF), *2018 Joint Propulsion Conference, American Institute of Aeronautics and Astronautics*, Cincinnati, Ohio, 2018. DOI: 10.2514/6.2018-4683

Broumand, M. and Birouk, M., Liquid jet in a subsonic gaseous crossflow: Recent progress and remaining challenges, *Progress in Energy and Combustion Science*, vol. 57, pp. 1–29, 2016. DOI: 10.1016/j.pecs.2016.08.003.

Brown, D.J. and Hutchinsan, P., The interaction of solid or liquid particles and turbulent fluid flow field – A numerical simulation, *Journal of Fluids Engineering*, vol. 101, pp. 265-269, 1979. DOI:10.1115/1.3448949

Brown, C.T., Mondragon, U.M., McDonell, V.G. and Hills, L., Investigation of the Effect of Injector Discharge Coefficient on Penetration of a Plain Liquid Jet into a Subsonic Crossflow, *ILASS Americas, 20th Annual Conference on Liquid Atomization and Spray Systems*, Chicago, Illinois, p. 11, 2007.

Crowe, C.T., Sommerfeld, M., and Tsuji, Y., Multiphase Flows with Droplets and Particles, Florida; *CRC Press*, 1998.

Dukowicz, J.K., A particle-fluid numerical model for liquid sprays, *Journal of Computational Physics*, vol. 35, nos. 2, pp. 229-253, 1980. DOI:10.1016/0021-9991(80)90087-X.

Elshamy, O. and Jeng, SM., Study of liquid jet in crossflow at elevated ambient pressures, *ILASS Americas, 18th Annual Conference on Liquid Atomization and Spray Systems*, California, Irvine, 2005.

Farvardin, E., Johnson, M., Alaee, H., Martinez, A. and Dolatabadi, A., Comparative Study of Biodiesel and Diesel Jets in Gaseous Crossflow, *Journal of Propulsion and Power*, vol. 29, pp. 1292–1302, 2013. DOI: 10.2514/1.B34743

Freitag, S. and Hassa, C., Spray characteristics of a kerosene jet in cross flow of air at elevated pressure. Spray characteristics of a kerosene jet in cross flow of air at elevated pressure, *ILASS Europe, 12th Annual Conference on Liquid Atomization and Spray Systems*, Como Lake, Italy, pp. 1-7, 2008.

Gorokhovski, M., and Oruganti, S., Stochastic models for the droplet motion and evaporation in under-resolved turbulent flows at a large Reynolds number, *Journal of Fluid Mechanics*, vol. 932, 2021. DOI:10.1017/jfm.2021.916

Gorokhovski, M.A. and Saveliev, V.L., Analyses of Kolmogorov's model of breakup and its application into Lagrangian computation of liquid sprays under air-blast atomization, *Physics of Fluids*, vol. 15, pp. 184–192, 2003. DOI: 10.1063/1.1527914

Gorokhovski, M., Zamansky, R., Le Ribault, C., and Deng, T., Application of stochastic models to primary air-blast atomization and cavitation, *Center for Turbulence Research Proceedings of the Summer Program 2012*, Stanford University, pp.325-334. 2012.

Gosman, A.D. and Ioannides, E., Aspects of computer simulation of liquid-fuelled combustors, *Journal of Energy*, vol. 7, nos. 6, 1981. DOI:10.2514/3.62687

Heide, J., Karlsson, M. and Altimira, M., Numerical Analysis of Urea-SCR Sprays under Cross-Flow Conditions. WCX^{TM} 17: *SAE World Congress Experienc*e, vol.1, pp. 2017-01–0964. 2017. DOI: 10.4271/2017-01-0964

Herrmann, M., Detailed Simulations of the Breakup Processes of Turbulent Liquid Jets in Subsonic Crossflows, *ICLASS 2009, 11th Triennial International Annual Conference on Liquid Atomization and Spray Systems*, 2009.

Huh, K.Y., and Gosman, A.D. A Phenomenological Model of Diesel Spray Atomization, *International Conference on Multiphase Flow*, Tsukuba, Japan, 1991.

Jangi, M., Solsjo, R., Johansson, B. and Bai, X., On large eddy simulation of diesel spray for internal combustion engines, *International Journal of Heat and Fluid Flow*, vol. 53, pp. 68-80, 2015. DOI: 10.1016/j.ijheatfluidflow.2015.02.002.

Johnson, P., and Meneveau, C., Predicting viscous-range velocity gradient dynamics in large-eddy simulations of turbulence, *Journal of Fluid Mechanics*, vol. 837, pp. 80-114, 2017. DOI:10.1017/jfm.2017.838

Jongen, T. Simulation and Modeling of Turbulent Incompressible Flows, *PhD*, Lausanne EPFL, 1998.

Karagozian, A. R. Transverse jets and their control, *Progress in Energy and Combustion Science*, vol. 36, no. 5, pp. 531–553, 2010. DOI: 10.1016/j.pecs.2010.01.001.

Kuo, K. K., and Acharya, R., Fundamentals of turbulent and multiphase combustion. United States; *Wiley*, pp. 576-721, 2012.

Lefebvre, A.H. and McDonell, V.G*, Atomization and sprays*, CRC Press, 2nd edition, pp.62, 2017.

Li, L., Lin, Y., Xue, X., Gao, W. and Sung, C.-J., Injection of Liquid Kerosene Into a High-Pressure Subsonic Air Crossflow From Normal Temperature to Elevated Temperature, *Combustion, Fuels and Emissions, vol. 2*, Copenhagen, Denmark, pp. 877–884. DOI: 10.1115/GT2012-69241

Li, X. and Soteriou, M., High-fidelity simulation of fuel atomization in a realistic swirling flow injector, *Atomization and sprays*, vol. 23, pp. 1049–1078, 2013. DOI: 10.1615/AtomizSpr.2013007395

Li, X., Soteriou and M.C., Detailed numerical simulation of liquid jet atomization in crossflow of increasing density. *International Journal of Multiphase Flow*, vol. 104, pp. 214–232, 2018. DOI:10.1016/j.ijmultiphaseflow.2018.02.016

Liu, A.B., Mather, D., and Reitz, R.D. Modeling the Effects of Drop Drag and Breakup on Fuel Sprays, *SAE Technical Paper* 930072, 1993. DOI: 10.4271/930072

Lubarsky, E., Reichel, J.R., Zinn, B.T. and McAmis, R., Spray in Crossflow: Dependence on Weber Number. *Journal of Engineering for Gas Turbines and Power*, vol. 132, no. 021501, 2010. DOI: 10.1115/1.2904892

Lubarsky, E., Shcherbik, D., Bibik, O., Gopala, Y. and Zinn, B.T., Fuel Jet in Cross Flow - Experimental Study of Spray Characteristics, *Advanced Fluid Dynamics*, pp.62-80, 2011. DOI: 10.5772/26045

Madabhushi, R.K., Leong, M.Y. and Hautman, D.J., Simulation of the Break-Up of a Liquid Jet in Crossflow at Atmospheric Conditions, *ASME Turbo Expo 2004: Power for Land, Sea, and Air, ASMEDC*, Vienna, Austria, vol. 1, pp. 697–704, 2004. DOI: 10.1115/GT2004-54093

Mahesh, K. The interaction of jets with crossflow, *Annual Review of Fluid Mechanics*, vol. 45, no. 1, pp. 379–407, 2013. DOI: 10.1146/annurev-fluid-120710-101115

Munson, B. R., Young, D. F. and Heubsch, W. W., Fundamentals of Fluid Mechanics, United States ; Wiley , pp.383-461, 2006.

Ničeno, B., Dhotre M.T. and Deen N.G., One-equation sub-grid scale (SGS) modelling for Euler–Euler large eddy simulation (EELES) of dispersed bubbly flow, *Chemical Engineering Science*, vol. 63, nos. 15, pp 3923-3931, 2008.

Nicoud, F. and Ducros, F., Subgrid-Scale Stress Modelling Based on the Square of the Velocity Gradient Tensor, *Flow, Turbulence and Combustion*, vol. 62, pp. 183-200, 1999. DOI:10.1023/A:1009995426001

Nihasigaye, P.B., Zhou, G. and Yang, X., Modelling spray performance of alternative aviation fuel, *Energy*, vol. 224, pp.1200-1286, 2021. DOI: 10.1016/j.energy.2021.120086

O'Rourke, P.J. and Amsden, A.A., The Tab Method for Numerical Calculation of Spray Droplet Breakup, *SAE International Fall Fuels and Lubricants Meeting and Exhibition, SAE Technical Paper 872089*, 1987. DOI: 10.4271/872089

Peszyński, K., Building a bridge between industry and theory on the example of a new ventilation system. *EPJ Web Conf*, vol. 213, 2019. DOI: 10.1051/epjconf/201921301001

Pilch, M. and Erdman, C.A., Use of breakup time data and velocity history data to predict the maximum size of stable fragments for acceleration-induced breakup of a liquid drop, *International Journal of Multiphase Flow*, vol. 13, nos. 6, pp.741–757, 1987. DOI: 10.1016/0301-9322(87)90063-2

Ragucci, R., Bellofiore, A. and Cavaliere, A., Trajectory and momentum coherence breakdown of a liquid jet in high-density air crossflow, *Atomization and Sprays,* vol. 17, nos. 1, pp. 47-70, 2007. DOI: 10.1615/AtomizSpr.v17.i1.20

Reitz, R. and Diwakar, R., Structure of High-Pressure Fuel Sprays, *SAE Technical Paper 870598,* 1987. DOI: 10.4271/870598

Rodi, W., Experience with Two-Layer Models Combining the k-e Model with a One-Equation Model Near the Wall, *American Institute of Aeronautics and Astronautics, 29th Aerospace Sciences Meeting,* United-States, Reno, NV, 1991. DOI: 10.2514/6.1991-216

Shih, T.-H., Liou, W.W., Shabbir, A., Yang, Z. and Zhu, J. A New k-epsilon Eddy Viscosity Model for High Reynolds Number Turbulent Flows - Model Development and Validation, *Computers & Fluids*, vol. 24, nos. 3,

pp. 227-238, 1995. DOI: 10.1016/0045-7930(94)00032-T.

Smagorinsky, J. General Circulation Experiments with the Primitive Equations: Part I, The Basic Experiment. *Monthly Weather Review*, vol. 91, pp. 99-164. 1963. DOI: /10.1175/1520-0493(1963)091<0099:GCEWTP>2.3.CO;2

Siemens Digital Industries Software., *Simcenter STAR-CCM+ 2020: User Guide*, Texas, USA, Siemens, accessed 2020-2021, from https://support.sw.siemens.com/en-US/product/226870983/download/PL20201113103827399, 2020.

Song, J., Cain, C.C. and Lee, J.G., Liquid jets in subsonic air crossflow at elevated pressure, *Journal of Engineering for Gas Turbine and Power*, vol. 137, 2014. DOI: 10.1115/1.4028565

Song, Y., Hwang, D. and Ahn, K., Effect of Orifice Geometry on Column Trajectories of Liquid Jets in Crossflows*, International Journal of Aeronautical and Space Sciences*, vol. 20, pp. 139–149, 2019. DOI: 10.1007/s42405-018-0130-3

Stenzler, J., Lee, J. and Santavicca, D., Penetration of Liquid Jets in a Crossflow, in: 41st Aerospace Sciences Meeting and Exhibit. *41st Aerospace Sciences Meeting and Exhibit, American Institute of Aeronautics and Astronautics*, Reno, Nevada, 2003. DOI: 10.2514/6.2003-1327

Tambe, S., Jeng, S., Mongia, H. and Hsiao, G., Liquid jets in subsonic crossflow, in: 43rd Aerospace Sciences Meeting and Exhibit. 43rd Aerospace Sciences Meeting and Exhibit, American Institute of Aeronautics and Astronautics, Reno, Nevada, 2005. DOI: 10.2514/6.2005-731

Tanner, F., Liquid Jet Atomization and Droplet Breakup Modeling of Non-Evaporating Diesel Fuel Sprays, *SAE Technical Paper 970050*, 1997. DOI: 10.4271/970050.

Tsang, C., and Rutland, C.J., Effects of Sub-Grid Scale (SGS) Dispersion Modeling on Large-Eddy Simulation (LES) of Non-Evaporative and Evaporative Diesel Sprays, *ILASS Americas, 29th Annual Conference on Liquid Atomization and Spray Systems*, Atlanta, GA, 2017.

Van Driest, E. R. On Turbulent Flow Near a Wall, *Journal of the Aeronautical Sciences*, vol. 23, nos. 11, pp. 1007-1011, 1956. DOI: 10.2514/8.3713

Vreman, B., Geurts, B., and Kuerten, H. Realizability conditions for the turbulent stress tensor in Large Eddy Simulation, *Journal of Fluid Mechanics*, vol. 278, pp. 351-362, 1994. DOI: 10.1017/S0022112094003745

Wang, Q. and Squires, K.D., Large eddy simulation of particle deposition in a vertical turbulent channel flow, *International Journal of Multiphase Flow*, vol. 22, nos. 4, pp. 667-683, 1996. DOI: 10.1016/0301-9322(96)00007-9.

Wen, J., Hu, Y., Nakanishi, A. and Kurose, R., Atomization and evaporation process of liquid fuel jets in crossflows: A numerical study using Eulerian/Lagrangian method, *International Journal of Multiphase Flow*, vol. 129, 2020. DOI: 10.1016/j.ijmultiphaseflow.2020.103331

Wolfstein, M. The velocity and temperature distribution in one-dimensional flow with turbulence augmentation and pressure gradient, *International Journal of Heat and Mass Transfer*, vol. 12, pp. 301-318, 1969.

Yang, Y., He, G. and Wang, L., Effects of subgrid-scale modeling on Lagrangian statistics in large-eddy simulation, *Journal of Turbulence*, vol. 9, nos. 8, pp. 1-24, 2008. DOI: 10.1080/14685240801905360

Zghal, M., Sun, X., Gauthier, P.Q. and Sethi, V., Validation and Assessment of a numerical methodology for turbulent liquid fuel jets in high-speed crossflow, *ASME Turbo Expo 2022: Power for Land, Sea, and Air*, Rotterdam, Netherlands, vol. 2, nos. 3, pp.1-12, 2022. DOI: 10.1115/GT2022-83166

https://dspace.org/

Validation of a stochastic breakup model for turbulent jets in high-speed crossflow: assessment of turbulent interactions and sensitivity to boundary conditions

Zghal, Malika; Sun, Xiaoxiao; Gauthier, Pierre Q.; Sethi, Vishal

2023-04-01
Begell House
https://doi.org/10.1615/AtomizSpr.2023041220
Zghal M, Sun X, Gauthier PQ, Sethi V. (2023) Validation of a stochastic breakup model for turbulent jets in high-speed crossflow: assessment of turbulent interactions and sensitivity to boundary conditions. Atomization and Sprays, Volume 33, Issue 4, April 2023, pp. 25-54

Downloaded from a DSpace repository. https://dspace.org/